Contract No:

This document was prepared in conjunction with work accomplished under Contract No. DE-AC09-08SR22470 with the U.S. Department of Energy (DOE) Office of Environmental Management (EM).

Disclaimer:

DESTRUCTIVE EXAMINATION OF SHIPPING PACKAGE 9975-02644

W. L. Daugherty

October 2017

SRNL-STI-2017-00666, Revision 0

DISCLAIMER

Printed in the United States of America

Prepared for
U.S. Department of Energy

SRNL-STI-2017-00666
Revision 0

Keywords: *K-Area*
Surveillance
9975 Shipping Package

Retention: *Permanent*

DESTRUCTIVE EXAMINATION OF SHIPPING PACKAGE 9975-02644

W. L. Daugherty

October 2017

Prepared in conjunction with work accomplished under contract number DE-AC09-08SR22470 with the U.S. Department of Energy (DOE) Office of Environmental Management (EM).

DESTRUCTIVE EXAMINATION OF SHIPPING PACKAGE 9975-02644

APPROVALS:

W. L. Daugherty _____ Date _____
Author, Materials Science and Technology

T. E. Skidmore _____ Date _____
Technical Review, Materials Science and Technology

B. L. Garcia-Diaz _____ Date _____
Pu Surveillance Program Lead, Materials Science and Technology

K. E. Zeigler _____ Date _____
Manager, Materials Science and Technology

R. J. Grimm _____ Date _____
NMM Engineering

REVIEWS:

D. R. Leduc _____ Date _____
Savannah River Packaging Technology

J. W. McEvoy _____ Date _____
9975 Shipping Package Design Authority

Summary

Destructive and non-destructive examinations have been performed on the components of shipping package 9975-02644 as part of a comprehensive SRS surveillance program for plutonium material stored in the K-Area Complex (KAC). During the field surveillance inspection of this package in KAC, three non-conforming conditions were noted: the axial gap of 1.389 inch exceeded the 1 inch maximum criterion, the exposed height of the lead shield was greater than the 4.65 inch maximum criterion, and the difference between the upper assembly inside height and the exposed height of the lead shield was less than the 0.425 inch minimum criterion. All three of these observations relate to axial shrinkage of the lower fiberboard assembly. In addition, liquid water (condensation) was observed on the interior of the drum lid, the thermal blanket and the air shield.

This package was subsequently transferred to SRNL for more detailed inspection and destructive examination. Condensation was no longer present in the package, but the following additional conditions were noted:

- Numerous small spots of corrosion were observed on the drum: along the bottom edge and side, on the inner surface, and on the bottom. None of these spots were observed to penetrate throughwall, but some did have pitting under the corrosion product.
- The shield inside diameter at the top (7.27 inches) exceeds drawing tolerances (7.25 – 7.26 inches).
- A musty odor was apparent when the lower fiberboard subassembly was removed, and mold was present around the bottom of the lower subassembly.
- The axial gap had increased slightly from 1.389 inches to 1.444 inches.

Several factors can contribute to the concentration of moisture in the fiberboard, including higher than average initial moisture content, higher internal temperature (due to internal heat load and placement within the array of packages), and the creation of additional moisture as the fiberboard begins to degrade. The concentration and distribution of moisture within the fiberboard can create temporary changes in fiberboard properties as well as permanent degradation.

Some degradation has likely occurred in the 9975-02644 fiberboard assembly, based on comparison of physical and mechanical properties to the average behavior of prior destructively examined packages and laboratory data. This is consistent with expectations based on the high internal heat load and period of storage it experienced. Evidence of fiberboard degradation is seen in compression test data and in the fiberboard height. However, since the initial fiberboard conditions are unknown, the specific contributions from degradation and from moisture re-distribution cannot be separated. Nevertheless, the rate of apparent decrease in properties due to degradation appears to be less than assumed in recent calculations to justify a storage period of 20 years. Accordingly, the condition of this package does not appear to compromise its capability to perform required safety functions for up to 20 years in storage.

The observed conditions must be fully evaluated by KAC to ensure the safety function of packages in storage is being maintained.

Introduction

The Savannah River Site (SRS) stores packages containing plutonium (Pu) materials in the K-Area Complex (KAC). The Pu materials are packaged per the DOE 3013 Standard and stored within Model 9975 shipping packages in KAC.

The KAC facility DSA (Documented Safety Analysis) [1] credits the Model 9975 package to perform several safety functions, including containment, criticality prevention, and fire resistance to prevent release of Pu/U oxide and metal materials. The Model 9975 package with a 3013 container is expected to perform its safety function for at least 20 years in the storage environment [2, 3]. Model 9975 packages with a non-3013 container are currently limited to 15 years storage. The DSA recognizes the degradation potential for the materials of package construction over time in the KAC storage environment and requires an assessment of materials performance to validate the assumptions of the analysis. This assessment is documented in the SRS Site Surveillance Program which is used to monitor material performance in order to establish a basis for the service life.

As part of the Site Surveillance Program [4-5], destructive examination of package 9975-02644 was performed following field surveillance in accordance with Reference 6. Field surveillance of the Model 9975 package in KAC included nondestructive examination of the drum, fiberboard, lead shield and containment vessels [5, 7]. Results of the field surveillance are summarized in Attachment 1.

Package History

Package 9975-02644 was loaded with plutonium oxide material at Hanford in accordance with DOE-STD-3013 and received into KAC in November 2007. The contents generated 16.5 watts heat load. Routine field surveillance was performed on July 6, 2017 after 9.6 years. After transfer to SRNL, DE examination activities were performed between August 2 and September 25, 2017.

Discussion

The results of the field surveillance [8] were reviewed. The following items were noted in the field surveillance:

- The exposed height of the lead shield was greater than the 4.65 inch maximum criterion.
- The difference between the upper assembly inside height and the exposed height of the lead shield was less than the 0.425 inch minimum criterion.
- The axial gap (1.389 inch) exceeded the 1 inch maximum criterion.
- Although the surveillance report noted as satisfactory that the drum was free from corrosion, photographs taken at the time show small spots of corrosion along the bottom lip of the drum (Figure 1). In addition, photographs of the drum interior show water stains along with areas that were later identified as light corrosion (Figure 2).

The first three observations noted in the field surveillance relate to shrinkage of the lower fiberboard assembly height. The lower assembly is not removed for measurement during field surveillance, but during subsequent laboratory measurements, the total height of the lower assembly was 0.65 inch less than nominal, and the lower assembly height above the bearing plate was 0.37 inch less than nominal. Compaction of the bottom layers results directly in a matching increase in the axial gap. As the sidewall region shrinks, more of the lead shield is exposed above the lower fiberboard assembly. Initially, this allows the upper assembly to drop (further increasing the axial gap), but once the upper assembly is resting on the shield lid, further sidewall region shrinkage leads to a gap between the upper and lower fiberboard assemblies.

It was also noted during field surveillance that water droplets were present on the underside of the drum lid (Figure 3a) and on top of the thermal blanket. In addition, field surveillance photographs show water on the side of the upper assembly air shield (Figure 3b). Condensation can occur in these areas after a package is moved from its warm storage location to a cooler room if the package contains elevated moisture levels. Elevated moisture levels can result from fiberboard degradation (water is a by-product of cellulose decomposition) or higher-than-average moisture could have been present when the package was first assembled.

As the package was first opened in SRNL and components removed, each component was marked to identify its orientation within the package. For components that were removed during the field surveillance, their orientation at the time of this examination has probably changed relative to that while stored in KAC. However, the lower fiberboard subassembly and lead shield would likely have remained in the same orientation they occupied in KAC.

Examination activities are documented through photographs, data sheets, and other documents. This documentation is maintained in a laboratory notebook [9]. The following examination activities were performed:

Fiberboard physical properties:

The weight and dimensions of the upper and lower fiberboard subassemblies were measured. The weight of the upper subassembly was 12.097 kg (26.67 lb). During the field surveillance, the measured weight of the upper subassembly was 26.6 lb. These two values are in good agreement. Weight and dimension data are recorded in Table 1.

The air shield was cut and peeled back at four locations to permit accurate measurement of the upper fiberboard subassembly dimensions. At three of these locations, some fiberboard remained stuck to the air shield. The average dimension UH1 reported in Table 1 is corrected for this fiberboard which separated from the assembly. In order to calculate the density of each subassembly, nominal dimensions were assumed for the air shield and aluminum bearing plates. The calculated densities (0.270 g/cc upper subassembly, 0.287 g/cc lower subassembly) meet the limit for the criticality control function, 0.20 g/cc minimum [6]. The volume and density were calculated using the following equations (see the Table 1 sketch for dimension nomenclature).

Upper subassembly fiberboard volume, $V_U = (UD1)^2\ (UH1)\ (\pi/4) + [(UD1) - 2\ (UR2)]^2\ (UH2)\ (\pi/4) - (UD2)^2\ (UH3)\ (\pi/4) - 59.96\ inch^3$

Upper subassembly fiberboard weight, W_U = upper subassembly weight – 9.773 lb
Upper subassembly fiberboard density, $\rho_U = W_U / V_U$
Lower subassembly fiberboard volume, $V_L = (LD1)^2 (LH1) (\pi/4) - [(LD2) + 2 (LR1)]^2 (LH3) (\pi/4) - (LD2)^2 (LH2) (\pi/4)$ – 59.96 inch^3
Lower subassembly fiberboard weight, W_L = bottom subassembly weight – 4.827 lb
Lower subassembly fiberboard density, $\rho_L = W_L / V_L$

Fiberboard dimensions measured during field surveillance are summarized in Attachment 1, and are generally consistent with drawing requirements and destructive examination measurements. For each of the dimensions measured in both the field surveillance and destructive examination, the measured values are similar. The dimensions were measured twice in SRNL, 27 and 40 days after the field surveillance.

The axial gap measured during field surveillance (1.389 inch) did not meet the specified 1 inch maximum criterion, and was slightly larger when measured in SRNL (1.444 inch). The increase likely resulted from additional fiberboard compaction during handling and transport. The as-built initial axial gap for this (or any other package) is unknown, but the nominal axial gap is specified as 0.8 inch. Changes in the fiberboard dimensions and the axial gap can occur from changes in the fiberboard moisture content, from settling and compaction during service, and from fiberboard degradation. Moisture accumulation in the bottom fiberboard layers can cause these layers to compress under the weight of the package internal components (shield and containment vessels) and the package contents. This is seen by comparing dimensions LH1 and LH2 in Table 1. Dimension LH1 (the full height of the lower fiberboard subassembly) is 0.654 inch below nominal, while dimension LH2 (height from the bearing plate to the lower subassembly lower step) is only 0.370 inch less than nominal. This indicates almost half of the reduction in height has occurred below the lower bearing plate. The remaining height reduction occurred in the sidewall region, and could have resulted from moisture loss or fiberboard degradation. Given the relatively high moisture content measured in this area, it seems likely that some degradation has occurred, since water is a byproduct of fiberboard degradation.

Fiberboard visual appearance:

A musty odor was noted when the lower fiberboard subassembly was removed and sectioned. Mold was observed near the bottom of the lower fiberboard subassembly, primarily along the glue joints (Figure 4). However, the mold generally appeared to be dormant, as evidenced by a lack of filaments and spore sacs on the surface. The bottom of the lower fiberboard subassembly contained a step, resulting from compaction against the step in the bottom of the drum (Figure 5). Inboard of the step, the bottom surface of the fiberboard is partially compressed in a ring about 2 inches wide, indicating this region was in partial contact with the drum bottom. Near this step (and generally within the 2 inch ring of partial contact) a water stain was observed, indicating the extent of penetration by liquid water (condensation on the top and sides of the drum, which ran down the sides to the bottom).

Despite the elevated moisture concentration at the bottom which can lead to swelling of the fiberboard, gaps existed between the lower fiberboard subassembly and drum, and the lower subassembly came out smoothly without interference.

Several locations on the lower fiberboard subassembly ID surface contained lead carbonate deposits from the shield. Figure 6 shows a region near the bottom of the ID surface with lead carbonate deposits from a rectangular feature on the shield. Figure 7 shows several areas of lead carbonate deposits, with the heaviest concentrations in a narrow band of 3 fiberboard layers. These three layers have a slightly different appearance, and generally feel slightly raised (i.e. a slightly smaller ID) which would contribute to closer contact with the shield. The heaviest deposit in this band is in a slight recess and matches a raised feature on the adjacent shield surface. It is likely that the fiberboard in this band was from a different production batch than the rest of the assembly. Most of the fiberboard assembly is constructed from sections that are pre-laminated to 2 inches thick. This one section was likely pre-fabricated separately and used to adjust the overall height of the assembly.

Fiberboard moisture content:

The moisture content of the fiberboard will affect its dimensions and properties, including density, mechanical strength and thermal properties. Measuring the moisture content of the upper and lower subassemblies, and the relative humidity inside the package, provides reference data to potentially correlate laboratory test results with behavior in KAC. The fiberboard moisture content was measured during the SRNL examinations. Measurements were also taken during field surveillance to the extent the fiberboard was accessible.

A GE Protimeter Surveymaster moisture probe was used to measure the moisture content of the upper and lower fiberboard subassemblies. This probe identifies the wood moisture equivalent (WME), or the weight % of moisture that would produce the same electrical conductivity in wood. Moisture content data from each examination are presented in Figure 8.

Moisture measurements were compared to those taken during previous destructive examinations. The fiberboard between the upper and lower bearing plates has an average moisture content of about 12 %WME, which is typical of the average moisture content seen in many packages. This average value remained about the same for both field surveillance and subsequent examinations, even though the moisture gradient decreased significantly. However, the fiberboard beyond the bearing plates has significantly higher moisture content (19 %WME at the top of the upper subassembly and over 20 %WME at the bottom of the lower subassembly). The fiberboard in this package may have been elevated to begin with, or moisture might have been created in the hotter regions as the fiberboard degraded over time (water is one of the decomposition products). Either way, a significant amount of moisture was re-distributed to the cooler regions after loading. The musty smell and presence of mold in the bottom fiberboard layers indicates that elevated moisture levels were present for a significant period of time. Elevated moisture levels near the outer fiberboard surface and bottom layers would have maintained equilibrium with a corresponding elevated level of relative humidity in the air between the fiberboard and drum. When the package was removed from storage for field surveillance, its transfer to a cooler (air conditioned) room would have caused the condensation observed on the underside of the lid and on the air shield. In addition, condensation could occur in storage each time the ambient temperature decreases significantly (i.e. summer to winter seasonal change).

Consistent with recent efforts to correlate moisture content of fiberboard with humidity in the surrounding air, these two parameters were measured. The fiberboard was placed back in the drum with a narrow channel cut down the side. A humidity probe was placed in this channel such that it could be raised and lowered. A plastic bag was taped over the top of the drum and sealed around the humidity probe cable. After allowing time for the humidity levels in the drum to approach equilibrium, humidity readings were taken at periodic elevations along the fiberboard, and the fiberboard was then removed to measure the moisture content at those same locations. The humidity data were then converted to the equivalent relative humidity corresponding to a constant temperature of 21 °C, since relative humidity is temperature dependent. These data are summarized in Figure 9, and compared to similar data from several previous DE packages and cane fiberboard laboratory samples. The data from 9975-02644 show reasonable agreement with the other data.

Fiberboard thermal and mechanical properties:

Samples of fiberboard were removed from the lower fiberboard subassembly to measure compressive strength (including energy absorption capacity), specific heat capacity and thermal conductivity. Figure 10 illustrates the locations from which these samples were removed. Physical data from the thermal conductivity and compression fiberboard samples are recorded in Table 2.

A total of four samples was prepared from the side and base of the lower subassembly for measuring the specific heat capacity of the fiberboard. The specific heat capacity was calculated in accordance with ASTM C351 at a mean temperature of ~25 ºC (77 ºF). This ASTM Standard specifies test temperatures that would produce a mean test temperature of 60 ºC, but allows alternate test temperatures to be substituted as needed. Data were collected for a sample target temperature of 45 ºC, and a water temperature of ~5 ºC. The average sample moisture content was 22.2 %WME for the two base samples and 9.4 %WME for the two side samples. Each sample was tested four times, and all results were averaged. The average specific heat capacity value was 1369 J/kg-K for the base samples, and 1124 J/kg-K for the side samples. The difference between these two averages reflects the different moisture content. Multiplying the specific heat capacity by the density of the lower subassembly (287 kg/m^3) and converting units gives a heat capacity of 6.09 Btu/ft^3-F for the base samples and 4.81 Btu/ft^3-F for the side samples. This meets the required minimum value of 3 Btu/ft^3-F. The specific heat capacity value is consistent with typical baseline laboratory data and previous DE packages, but falls near the bottom of the observed range.

The thermal conductivity sample from the bottom center of the lower subassembly is oriented for heat flow in the axial direction (perpendicular to the glue joints). The thermal conductivity sample from the side is oriented for heat flow in the radial direction (parallel to the glue joints). The thermal conductivity of the fiberboard was measured with either a Lasercomp Inc. Fox 300 or Fox 314 thermal conductivity instrument at a mean temperature of 25 ºC (77 ºF). For a nominal moisture content of ~10 %WME, thermal conductivity in the axial direction (perpendicular to the fiberboard layers) is 0.0363 Btu/hr-ft-ºF, and thermal conductivity in the radial direction (parallel to the fiberboard layers) is 0.0616 Btu/hr-ft-ºF. The axial orientation sample was also tested with higher moisture content since the top and bottom fiberboard layers

of this package had higher moisture content. The axial thermal conductivity is 0.0376 Btu/hr-ft-ºF at ~17 %WME and 0.0393 Btu/hr-ft-ºF at ~23 %WME. These values fall within the identified range [6], and are consistent with typical baseline laboratory data [10].

The compression test data are shown in Figures 11 and 12, along with baseline data for a different fiberboard assembly. A series of photographs showing typical compression behavior under parallel loading is shown in Figure 13. The area under the stress-strain curve up to 40% strain is used as a relative indication of the energy absorption capacity of the fiberboard. The buckling strength provides an additional comparison metric for samples tested in the parallel orientation.

Figures 14 and 15 compare compression test metrics from all the DE packages, plotted as a function of fiberboard moisture content. In these comparative figures, the 9975-02644 data are circled for identification. Energy absorption (Figure 14) tends to decrease with increasing moisture content. Figure 14 includes data from several DE packages that have not been previously reported. These samples were recently tested after conditioning in a humid environment to provide more comparative data at relatively high moisture content. The samples from 9975-02644 consistently fall near the bottom of the range for all DE packages. Comparable trends are seen for the buckling strength (obtained from compression samples tested in the parallel orientation) in Figure 15.

Fiberboard Degradation Assessment

Fiberboard properties can change over time due to several mechanisms:

- The cellulose structure can break down at elevated temperature due to thermo-oxidation processes. Reference 10 identifies a threshold of about 120 – 125 °F, below which this mechanism appears to be not significant, based on available aging data. With this mechanism, degradation rates tend to increase as the moisture level increases, and water is a decomposition product, so unless excess moisture can gradually escape, this mechanism can accelerate over time. Fortunately, the 9975 package is not air-tight and it allows limited air / moisture exchange with the surrounding environment. All properties are degraded by thermo-oxidation, although the degradation rates vary for specific properties. Any degradation resulting from thermo-oxidation processes is permanent, and will continue to accumulate so long as the elevated temperature environment is present. The hottest regions of fiberboard (most susceptible to this mechanism) are along the inner surface of the sidewall region, and directly below the lower bearing plate.
- If the fiberboard moisture content is sufficiently high, biological processes (e.g. mold) can consume the fiberboard. Limited data indicate mold will not grow above temperatures of ~125 °F, and elevated moisture will generally be found in the cooler bottom fiberboard layers. It is currently unknown how fast mold will consume the fiberboard, although packages in which mold has been identified have not displayed a noticeable loss of material to date.
- As the fiberboard moisture content changes, the properties will change. If the original moisture levels are restored, these changes are reversible, with some exceptions. If the moisture content of the bottom fiberboard layers increases significantly, the fiberboard will weaken and compress under the weight of the internal package components. If the moisture

level subsequently decreases, there may be minimal decompression, although the fiberboard strength can be restored.

The possibility of fiberboard degradation in the warmer sidewall region of 9975-02644 is examined as follows:

- The long-term average ambient temperature in KAC is 74 °F, with seasonal variation generally between 60 and 90 °F [11]. This reference also identified that a package within a storage array can have an effective ambient temperature 11 °F higher than the room ambient temperature, and that the net degradation rate for a component subject to this seasonally varying environment is approximately equivalent to the rate calculated for the average component temperature.
- At 19 watts, the maximum fiberboard sidewall temperature is 49 °F warmer than ambient temperature (based on the finite element model described in Reference 12).
- Adjusting for the package heat load of 16.5W, the average inner sidewall fiberboard temperature in 9975-02644 would have been 74 °F + 11 °F + 49 °F * (16.5W / 19W) = 128 °F. Since this temperature is above the identified threshold for degradation, some degradation might be expected.

Given the possibility of fiberboard degradation, predictions of degradation rate can be compared to actual observations, keeping in mind that the initial properties of the fiberboard are unknown and other factors can contribute to changes in fiberboard properties. Rates for degradation related to thermo-oxidation are available from Reference 10. Fiberboard changes related to moisture redistribution occur primarily as the moisture levels are changing, and then slow down significantly.

- At 125 °F (approximating 128 °F), along with low moisture content, the degradation model in Reference 10 predicts energy absorption will decrease by 80% (to 0.011 ksi) in about 242 years, giving an average rate of decrease of 0.33 %/year. At this degradation rate, the energy absorption of the inner sidewall fiberboard region in 9975-02644 is expected to have decreased about 3% over 9.6 years. Figure 14 compares the energy absorption data for the DE packages with baseline data from laboratory samples. Since the trendlines represent the average baseline behavior of the laboratory samples from which the Reference 10 degradation rate models were developed, they will be used as a comparison point for the DE package behavior. The average energy absorption of all 9975-02644 compression test samples is 3.7% less than the average of the respective laboratory sample trendline values. While there is significant variation between samples (from 23% below the laboratory sample trendline to 22% above the laboratory sample trendline), the large-scale average fiberboard behavior is most relevant to energy absorption in an impact scenario.

- The radial thermal conductivity sample (which was also removed from the inner sidewall region) gave results very comparable to the average behavior of other DE packages (Figure 16). The degradation rate for thermal conductivity in a low humidity 128 °F environment is predicted to be 0.034 %/year [10], so no discernible degradation would be expected for this parameter.

- The Reference 10 model for cane fiberboard height predicts 0.033 %/year axial shrinkage due to degradation at this storage environment. This leads to an expected height change of 0.06 inch for the lower assembly inside surface over the 9.6 year storage period. Such degradation accounts for a small part of the apparent loss of height (0.37 inch below nominal). The loss of moisture in this region likely contributed significantly to the decreased height, but rates for this mechanism have not been quantified.

- Measured radial and outside diametral dimensions are consistently slightly less than nominal, and inside diameters are slightly higher than nominal, suggesting some radial shrinkage may have occurred. The Reference 10 model for cane fiberboard radial dimensions predicts 0.011%/year shrinkage due to degradation in this storage environment. This corresponds to a change of 0.019 inch in the 18 inch diameter of the fiberboard assembly. However, the 128 °F temperature exists only along the ID surface, and most of the fiberboard bulk will experience significantly lower temperatures. Therefore, no detectable radial shrinkage is expected as a result of thermo-oxidation mechanisms. Regions of the fiberboard assembly that lost moisture while in storage would experience modest shrinkage. In contrast to these expectations, the lower assembly outside diameter is measured at the bottom where the temperature is close to ambient and the moisture levels are increased. These conditions should lead to an increased diameter, but this dimension was also slightly below nominal. Therefore, it is concluded that no significant change (from degradation or other causes) has occurred in the radial and diametral dimensions.

Lead shield examination:

The entire surface of the lead shield was visually examined. It was found to be free from significant deformation and physical damage. The outer side surface is covered with white corrosion product (Figure 17), as has been observed on other packages. The corrosion product was scraped away from 8 locations around the top edge, and the shield thickness was measured at these locations before and after scraping (Table 3). The difference provides an estimate of the corrosion product thickness, ranging from 0.005 to 0.015 inch.

The corrosion product thickness varied around the shield circumference, with the thinnest and thickest readings on opposite sides. At some locations, portions of the corrosion product had flaked off from handling before the initial measurements were made (where flaking has occurred, the remaining corrosion product is whiter in appearance). Measurements immediately adjacent to a flaked area indicate that minimal amounts had been removed. However, the locations with the thickest and thinnest corrosion product were measured with the full corrosion product thickness intact.

An upper bound estimate of the amount of metal consumed is provided by assuming that 0.45 mil of metal is lost for every mil of corrosion product [13, 14]. This relationship indicates that approximately 2 to 7 mils of metal was lost to corrosion. This gives an average corrosion rate of 0.7 mils/year or less. Reference [13] recommended a corrosion rate of 2 mils/year as a conservative estimate for 9975 packages. The calculated corrosion rate for this package is significantly less than this bounding value.

Several lead shield dimensions were measured (Table 4). One dimension (inner diameter at the top) exceeds the specified range. All other dimensions are consistent with drawing requirements.

The radial thickness was measured near the top of the shield, and was calculated from diametral data taken near the bottom of the shield. The calculated thickness from near the bottom (0.543 inch) is slightly less than the measured thickness near the top (0.574 inch). This comparison is made to indicate whether the lead may have undergone creep during service; and indicates no significant creep has occurred to date.

A band around the center of the shield is darker in color than the rest of the shield, indicating a thinner layer of corrosion product. This band corresponds to a three-layer section of the lower fiberboard assembly which is lighter in color than the rest of the assembly (Figure 7). Raised features within and near this band correspond to the heaviest lead carbonate deposits shown in Figure 7. The largest of these features on the shield had very little corrosion product remaining on it. An additional raised feature was observed on the lower side of the shield at ~90 degrees orientation (Figure 18) corresponding to the lead carbonate deposits seen in Figure 6. While this rectangular feature is similar in size to the four bolting lugs around the top of the shield, the specific cause of this feature was not identified.

O-ring examination and testing:

Prior surveillance testing of the four O-rings from this package included visual examination, dimensional and hardness measurements. Dimensional measurements were repeated on each O-ring as part of the destructive examination. Three of these O-rings (SCV outer, PCV outer and PCV inner) received additional testing. All three were submitted for FT-IR spectroscopy to confirm material composition, and the two outer O-rings received optical and SEM microscopic examination of the cross section. The dimensions and weight of the SCV outer and PCV outer O-rings were recorded to calculate their density. The PCV inner O-ring was tensile tested, including a hold point at 50% strain to visually examine the O-ring.

Weight and dimension data for the two outer O-rings are presented in Table 5. The average minor diameter for each O-ring is within the specified tolerances for new O-rings, but the major inside diameter for each O-ring (calculated from the length measured after the O-ring was cut) is greater than specified for new O-rings. This is consistent with a permanent stretch due to the lid diameter. Leak testing during the field surveillance successfully demonstrated leak-tightness to a level of approximately 1×10^{-3} std cc air/sec.

Compression set was calculated for each O-ring for each time the dimensions were measured. Compression set is calculated as follows, assuming an initial minor diameter of 0.139 inch and an average groove depth in the lid of 0.0995 inch.

$$\text{Compression set (\%)} = (0.139 - \text{radial thickness}) / (0.139 - 0.0995) * 100$$

Compression set for the 9975-02644 O-rings ranged from 13 to 36% based on KAC measurements. Compression set decreases with time, as the polymer continues to relax, and typically reaches an equilibrium value after about 30 days. When measured in SRNL 36 days

later, the compression set ranged from 0.3 to 21%. Individual readings for some O-rings varied significantly for the KAC and/or the SRNL measurements, suggesting the O-rings may have twisted after removal. The compression set values are generally consistent with the range of values measured for O-rings from other packages.

FT-IR spectroscopy generically identified the composition of each O-ring as consistent with a Viton® type fluoroelastomer (Figure 19). Each O-ring produced a similar FTIR spectrum consistent with that from previous characterization of Viton® GLT O-rings, and with a library image of a Viton® FTIR spectrum.

As with previous destructive examinations, visual (Figure 20) and SEM (Figure 21) examination of the cross sections identified a distribution of very small particles throughout each O-ring. Aside from carbon and fluorine (the primary constituents of Viton® fluoroelastomer) the SEM identified small amounts of zinc, aluminum, calcium and silicon. Though the actual compound is proprietary, Viton®-type fluoroelastomer compounds typically contain MgO, CaO, $Ca(OH)_2$, ZnO or lead compounds as acid acceptors and heat stabilizers [15]. Aluminum is present in hydrotalcite, which is used in both GLT and GLT-S compounds as a filler reinforcing agent. Silicon may be present as a trace contaminant.

The PCV inner O-ring was tensile tested in accordance with ASTM D1414, using a cut (single strand) sample. The test was interrupted at 50% strain (Figure 22) to visually examine the O-ring for signs of cracking or other degradation. None were observed. The test was performed twice, with different grip arrangements. With yarn grips, some additional stretch beyond the gage section is possible, especially if any grease remains on the O-ring, which causes the elongation to be over-reported. The elongation is measured more accurately with flat grips, but they pose a greater risk of breaking within the grips (which would invalidate the test). Therefore, the portion of O-ring within the flat grips was wrapped with tape for cushioning.

The stress-strain curve for the PCV inner O-ring tested with flat grips is shown in Figure 23, along with a baseline O-ring for comparison and results from other packages removed from service that were similarly tested. The O-ring failed after reaching 245% elongation, with a tensile strength of 1.8 ksi. These values are consistent with Viton GLT mechanical properties.

General:

A general visual examination was performed on all metallic components. No significant damage or degradation of the containment vessels was observed. Various fabrication markings were stamped or engraved on the containment vessels and lids. These markings appear to be identification numbers used during manufacture, prior to association of the parts with a final package number, and are consistent with those seen in other packages.

Corrosion was observed on the stainless steel drum and air shield in several locations, as follows:

- Several corrosion spots were observed on the rolled bottom edge of the drum (Figure 24) and in the crevice between the rolled bottom edge and drum side (Figure 25). Corrosion in or connected to this crevice may be related to moisture seeping through the rolled edge, and could signal additional internal corrosion. However, this corrosion does not appear as severe

as that observed previously on 9975-02101 [16]. The corrosion on the rolled edge that does not connect to the crevice is more likely caused by factors external to the package.

- Corrosion was observed on the drum OD side just above the stitch welds (Figures 24(c) and 26). The corrosion in Figure 24(c) is high enough above the rolled edge that the ID surface opposite this spot is accessible. No corrosion was observed on the ID surface at this location, indicating that the corrosion likely initiated from the outside. The ID surface opposite the corrosion in Figure (26) is not accessible.
- Small corrosion spots were observed on the bottom of the drum along the outer corner (Figure 27). These spots are superficial and are much less severe than observed previously on other packages [16, for example]. In addition, one spot of corrosion was observed on the drum bottom close to the center (Figure 28). Cleaning of this area was attempted by increasingly aggressive methods - wiping, brushing with a soft-bristle brush, and brushing with a wire brush. Each step removed additional material, with the wire brush removing essentially all corrosion product. Numerous small pits were observed under the corrosion product (Figure 29). No corrosion was observed on the drum interior opposite this spot, indicating that this corrosion also likely initiated from the outside.
- Numerous small corrosion spots were observed on the drum ID surface along with water staining (Figure 30). A portion of this area was cleaned by wire brushing. Most of the corrosion product was removed, but a degree of staining remained. No significant pitting was observable compared to the as-fabricated roughness of this ID surface.
- Several spots of corrosion were observed on the top of the air shield near the edge at 0 degree orientation (Figure 31). No evidence of pitting was observed after some of these spots were removed by brushing. Where the air shield was cut away to access the fiberboard, no corrosion was observed on the interior surface of the air shield.

As discussed above, the fiberboard moisture content is higher than in a typical package, and segregation of that moisture preferentially to the outer and bottom fiberboard regions makes it possible for condensation to occur whenever the ambient temperature drops (as with seasonal changes). While the condensation observed during field surveillance likely resulted from moving the package to a cooler location, similar condensation would have to have been present over an extended period to lead to the corrosion seen on the drum interior and air shield.

The data from the examination activities described above are compared with field surveillance data in Attachment 1. There is general agreement between the two examinations, although some differences are to be expected as moisture re-distributes within the fiberboard and the O-rings slowly relax. All findings will be reviewed by NMM for potential impact on the continued storage of other packages in KAC.

Measurement Uncertainties:

Numerous measurements were made with a variety of instruments during the destructive examination of package 9975-02644. Some of the measurements were specifically compared to inspection criteria, while others were taken for information / trending purposes. All measurements which are compared to inspection criteria were made with calibrated instruments, or were verified against calibrated instruments. The uncertainties associated with measurements and calculated results required to meet inspection criteria are discussed below.

Weight – The weight of each fiberboard subassembly was measured to a precision of 1 gram. The balance used was M&TE, and the calibration data show accuracy within 5 grams over the range of interest. A conservative net uncertainty of 6 grams will be used.

Calipers – Three different calipers were used to measure component dimensions. All three calipers are M&TE. Calibration data show accuracy within 0.001 inch for the 6 and 40 inch calipers and within 0.002 inch for the 24 inch calipers. In addition, operator bias can affect measurement accuracy through the contact load applied when making a measurement. A degree of give exhibited by the fiberboard will lead to different results as the contact load changes. The larger calipers are judged to be more susceptible to this bias. Metallic components are significantly more rigid than the fiberboard, but operator bias may also exist for those components. While not characterized explicitly, it is judged that the total uncertainty (instrument uncertainty plus operator bias) for fiberboard measurements is no greater than +/- 0.003 inch for the 6 inch calipers, +/- 0.006 inch for the 24 inch calipers, and +/- 0.007 inch for the 40 inch calipers. It is further judged that total uncertainty when measuring metallic components is no greater than +/- 0.003 inch for 6 inch calipers, and +/- 0.005 inch for the 24 and 40 inch calipers.

Manual calipers – Dimension ID2 on the lead shield was captured with manual swing calipers, which was then locked to that dimension and measured with 24-inch calipers. It is judged that the accuracy of capturing this dimension with the manual calipers is within +/- 0.002 inch, and the measurement of that dimension is then within +/- 0.002 inch, for a (conservatively) combined accuracy of +/- 0.004 inch.

Thermal conductivity instrument – The specifications for the Fox 300 and Fox 314 thermal conductivity instruments include a stated accuracy of ~1% and 2%, respectively. Measurement of the thermal conductivity of a calibration standard was accurate to within 1.1% on either instrument. An uncertainty of 3% will be conservatively assumed for the current measurements on either instrument.

Heat capacity – The specific heat capacity is derived from temperature and weight measurements, using calibrated instruments. The thermocouple and balance precisions are high. The greatest contribution to error in the specific heat capacity is considered to be consistency of operator technique. The total uncertainty is reflected in the range of results for multiple trials. The heat capacity was reported separately for the base and side regions, with four measurements on each of two samples from each region. The variation for each sample ranged from 11.8 to 36.3%. The combined uncertainty on the average of 2 samples is 9.2% for the base region, and 20.9% for the side region.

Where measurement results are used in subsequent calculations, the uncertainty values identified above are assumed to be random. A standard error propagation formula for random errors is used to calculate the final result uncertainty. In some cases, the calculated uncertainty may be less than the potential error from rounding off the result, and the higher variation associated with round-off is reported as the uncertainty. These calculations are documented in the Laboratory Notebook [9]. Calculation results and their uncertainties are summarized as follows:

- Upper fiberboard subassembly volume = 28404 +/- 29 cm^3
- Upper fiberboard subassembly density = 0.270 +/- 0.001 g/ cm^3
- Lower fiberboard subassembly volume = 83585 +/- 83 cm^3
- Lower fiberboard subassembly density = 0.287 +/- 0.001 g/ cm^3
- Shield radial thickness at bottom = 0.543 +/- 0.003 inch
- Thermal conductivity (radial) = 0.0616 +/- 0.002 Btu/hr-ft-ºF
- Thermal conductivity (axial) = 0.0393 +/- 0.001 Btu/hr-ft-ºF
- Heat capacity = 4.8 +/- 1.0 Btu/ft^3-ºF (side), 6.1 +/- 0.6 Btu/ft^3-ºF (base)

References

[1] WSRC-SA-2002-00005, Rev. 12, "K-Area Complex Documented Safety Analysis", March 2017.

[2] M-ESR-K-00073, "Evaluation of 9975 Shipping package Analyses For 20 Year Storage of 3013 Containers In KAC", S. J. Hensel, March, 2017.

[3] G-ESR-K-00204, "9975 Shipping Package 20 Year Life Extension Summary", R. J. Grimm, May, 2017

[4] SRNS-TR-2008-00290, Revision 2, Summary and Matrix for the 9975 Shipping Package Qualification Programs for Extended Storage of Plutonium in the K-Area Complex (U), August 2016

[5] WSRC-TR-2001-0286, Rev. 9, "The Savannah River Site Surveillance Program for the Storage of 9975/3013 Plutonium Packages in KAC", October 2017

[6] WSRC-TR-2005-00135 Rev. 1, "Task Technical and Quality Assurance Plan for Destructive Examination of a 9975 Package from Field Surveillance Activities", W. L. Daugherty, March 2011

[7] WSRC-TR-2004-00197 Rev. 1, "Inspection Activities and Acceptance Criteria for Field Surveillance of Model 9975 Package O-Rings and Celotex® Materials", W. L. Daugherty, October 2005

[8] SOP-CSS-231-K, Rev. 6, Attachment 8.5 "3013/9975 Surveillance Data Sheet" for 9975-02644, July 6, 2017

[9] SRNL-NB-2012-00048, Laboratory Notebook "9975 Shipping Package Celotex Testing Book IV", and SRNL-NB-2017-00009, Laboratory Notebook "9975 Shipping Package Celotex Testing Book IV"

[10] SRNL-STI-2015-00610, "Status Report – Cane Fiberboard Properties and Degradation Rates for Storage of the 9975 Shipping Package in KAC", W. L. Daugherty, December 2015

[11] SRNL-STI-2015-00441, “Temperature Environment for 9975 Packages Stored in KAC”, W. L. Daugherty, September 2015

[12] M-CLC-K-00788, “The Initial and 20-year Service Thermal Performances of the 9975 Shipping Packages due to Fire-Drop-Smoldering Accidents in KAC”, B. B. Kiflu, January 17, 2017

[13] WSRC-TR-2006-00094, “Corrosion of Lead Shielding in Model 9975 Package”, K. H. Subramanian, March 2006.

[14] SRNL-STI-2017-00514, “Examination of Shipping Package 9975-04985”, W. L. Daugherty, August 2017

[15] Rubber Technology Handbook, W. Hofmann, Hanser Publishers, New York, 1989, page 122

[16] SRNL-STI-2016-00209, Destructive Examination of Shipping Package 9975-02101”, W. L. Daugherty, May 2016

Table 1. Fiberboard physical measurements and calculated density

Upper Subassembly						
Weight	12.097 kg					R-R2-F-0019 Rev 5
	0/180 deg.		90/270 deg.		Avg.	Nominal value (inch)
UD1 (in)	17.658		17.634		17.646	17.7
UD2 (in)	8.562		8.564		8.563	8.55
	0 deg.	90 deg.	180 deg.	270 deg.	Avg.	
UR1 (in)	3.037	3.034	3.034	3.040	3.036	3.075
UR2 (in)	1.502	1.499	1.472	1.428	1.475	1.5
UH1 (in)	7.075	6.992	7.068	7.026	7.072*	7.1
UH2 (in)	2.077	2.070	2.058	2.085	2.075	2.1
UH3 (in)	4.977	5.010	5.019	5.012	5.004	5.0

* Dimension UH1 average is corrected by 0.032” for fiberboard stuck to air shield.
Upper subassembly calculated density = 0.270 g/cc

Lower Subassembly						
Weight	26.140kg					R-R2-F-0019 Rev 5
	0/180 deg.		90/270 deg.		Avg.	Nominal value (inch)
LD1 (in)	18.032		18.026		18.029	18.1
LD2 (in)	8.496		8.497		8.496	8.45
	0 deg.	90 deg.	180 deg.	270 deg.	Avg.	
LR1 (in)	3.210	3.237	3.255	3.262	3.241	3.275
LR2 (in)	1.506	1.514	1.507	1.511	1.510	1.55
LH1 (in)	26.042	26.074	26.020	26.048	26.046	26.7
LH2 (in)	20.023	20.050	20.035	20.011	20.030	20.4
LH3 (in)	1.989	1.994	2.019	2.016	2.004	2.0

Lower subassembly calculated density = 0.287 g/cc

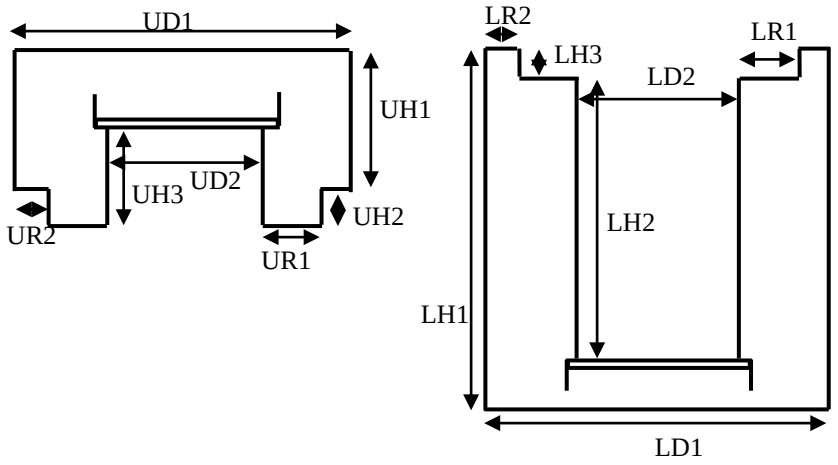

Table 2. Physical data for fiberboard test specimens

Test Sample	Moisture Content (%WME)	Weight (g)	Length (inch)	Width (inch)	Height (inch)	Density (g/cc)
Compression Test Samples						
Side 1 (parallel)	10.0	35.170	1.997	1.995	1.995	0.270
Side 2 (parallel)	10.2	33.826	1.986	1.975	1.992	0.264
Side 3 (perpendicular)	9.8	34.301	1.982	1.983	1.982	0.269
Side 4 (perpendicular)	9.8	35.376	1.962	1.990	1.994	0.277
Side 5 (perpendicular)	9.8	34.220	1.960	1.986	1.993	0.269
Base 1 (perpendicular)	24.3	38.959	1.994	2.060	2.030	0.285
Base 2 (parallel)	27.5	39.542	1.996	2.049	2.046	0.288
Base 3 (parallel)	17.7	36.230	1.985	2.053	1.985	0.273
Base 4 (parallel)	14.7	36.444	1.991	2.043	1.985	0.275
Base 5 (perpendicular)	14.1	36.082	1.991	2.039	1.988	0.273
Base 6 (perpendicular)	14.7	36.483	1.991	2.041	1.991	0.275
Thermal Conductivity Samples						
Side (radial)	10.2	362	7.089	6.942	1.649	0.272
Base (axial) *	23.1	352	6.827	7.087	1.556	0.285
	16.6	344	6.818	7.084	1.545	0.281
	10.4	336	6.798	7.064	1.530	0.279

* Data provided for the axial thermal conductivity sample at three different moisture levels.

Table 3. Determination of corrosion product thickness on the lead shield by measuring the shield radial thickness before and after scraping away the corrosion product

Position	Initial Radial Thickness (inch)	Radial Thickness after Scraping (inch)	Corrosion Product Thickness (inch)	Metal Consumed by Corrosion (inch)	Original Metal Thickness (inch)
0 deg	0.585 *	0.573	0.012	0.005	0.578
45 deg	0.579	0.564	0.015	0.007	0.570
90 deg	0.577 *	0.563	0.014	0.006	0.569
135 deg	0.582 *	0.570	0.012	0.005	0.575
180 deg	0.553 *	0.544	0.009	0.004	0.548
225 deg	0.577	0.572	0.005	0.002	0.574
270 deg	0.581	0.573	0.008	0.004	0.576
315 deg	0.585	0.578	0.007	0.003	0.581

* At these locations, a small portion of the corrosion product flaked off during handling before measurement.

Measurement location at 45 deg (at arrows)

Table 4. Lead shield dimensions

Dimension	0/180 deg. (inch)		90/270 deg. (inch)		Avg. (inch)	Requirement (inch)
OD (in)	8.339		8.348		8.344	8.252 – 8.35
ID1 (in)	7.283		7.258		7.270*	7.25 – 7.26
ID2 (in)	7.253		7.262		7.258	7.24 – 7.26
	0 deg.	90 deg.	180 deg.	270 deg.		
R (in)	0.584	0.576	0.556	0.582	0.574	0.506 min
H (in)	24.682	24.668	24.675	24.681	24.676	24.556 – 24.7

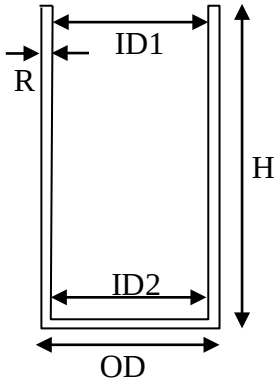

(OD – ID2) / 2 = 0.543 inch

* ID1 re-measured at 4 locations, average value = 7.273 inch

Table 5. O-ring physical data

36 Days after Field Surveillance	PCV Outer O-Ring Thickness		SCV Outer O-Ring Thickness	
	Radial (inch)	Axial (inch)	Radial (inch)	Axial (inch)
Minor Dia. 0 deg	0.1355	0.1350	0.1410	0.1365
Minor Dia. 45 deg	0.1340	0.1370	0.1400	0.1370
Minor Dia. 90 deg	0.1340	0.1375	0.1390	0.1370
Minor Dia. 135 deg	0.1345	0.1375	0.1380	0.1365
Minor Dia. 180 deg	0.1370	0.1370	0.1390	0.1355
Minor Dia. 225 deg	0.1360	0.1325	0.1380	0.1285
Minor Dia. 270 deg	0.1380	0.1320	0.1385	0.1285
Minor Dia. 315 deg	0.1375	0.1350	0.1380	0.1300
Average Thickness	**0.1358**	**0.1354**	**0.1389**	**0.1337**
Minor Dia. (new)	0.139 +/- 0.005 inch		0.139 +/- 0.005 inch	
Length (after cut)	13 31/32 inch		17 9/32 inch	
Calculated Major Dia.	4.446 inch avg		5.501 inch avg	
Major Inside Dia. (new)	4.234 +/- 0.045 inch		5.234 +/- 0.054 inch	
Weight	5.9599 g		7.2546 g	
Calculated Volume	0.2026 $inch^3$ (3.320 cm^3)		0.2521 $inch^3$ (4.132 cm^3)	
Calculated Density	**1.795 g/cm^3**		**1.756 g/cm^3**	

	PCV Inner O-Ring Thickness		SCV Inner O-Ring Thickness	
	Radial (inch)	Axial (inch)	Radial (inch)	Axial (inch)
Minor Dia. 0 deg	0.1325	0.1375	0.1305	0.1365
Minor Dia. 45 deg	0.1405	0.1340	0.1295	0.1365
Minor Dia. 90 deg	0.1390	0.1325	0.1300	0.1360
Minor Dia. 135 deg	0.1390	0.1325	0.1315	0.1360
Minor Dia. 180 deg	0.1400	0.1315	0.1325	0.1360
Minor Dia. 225 deg	0.1395	0.1315	0.1310	0.1365
Minor Dia. 270 deg	0.1400	0.1315	0.1305	0.1375
Minor Dia. 315 deg	0.1365	0.1365	0.1310	0.1375
Average Thickness	**0.1384**	**0.1334**	**0.1308**	**0.1366**

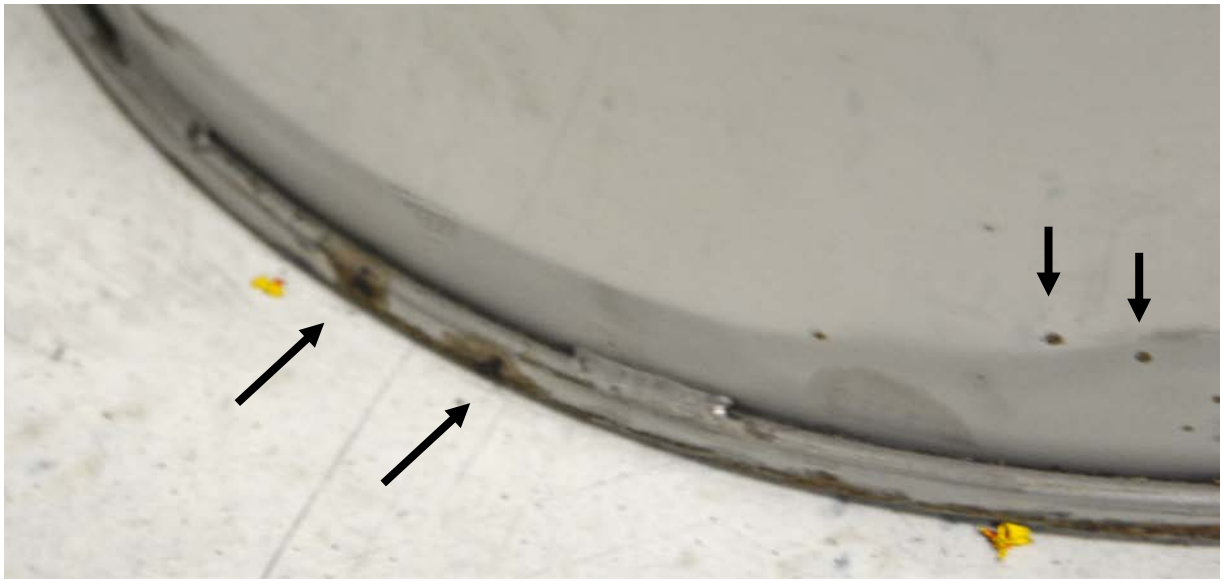

(a)

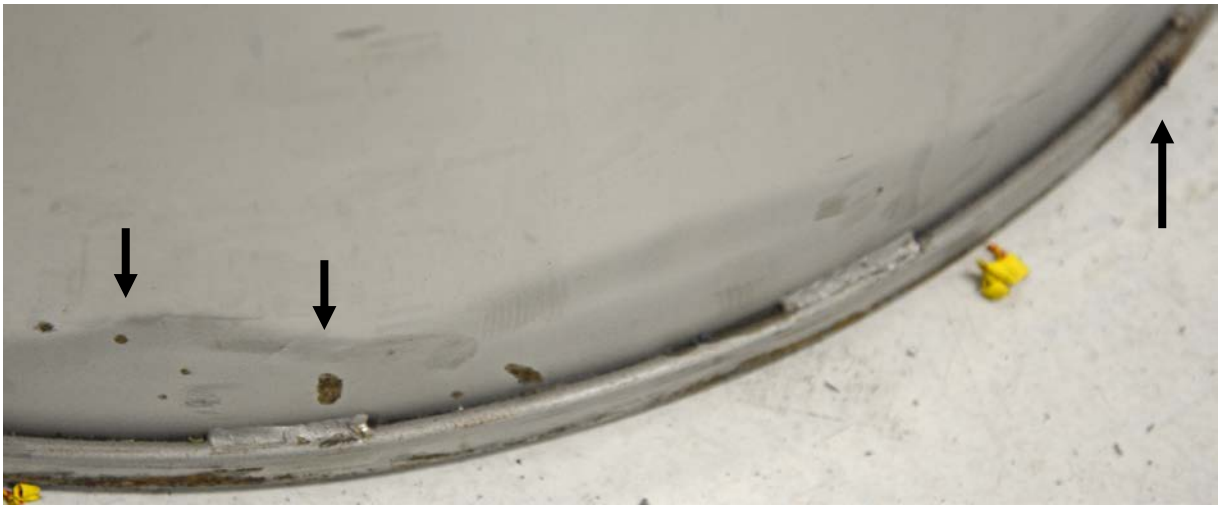

(b)

Figure 1. Corrosion observed along the bottom lip of the drum during field surveillance. Photographs taken by KAC personnel.

Figure 2. Staining on the drum interior with areas that were later identified as light corrosion. Photograph taken by KAC personnel during field surveillance.

(a)

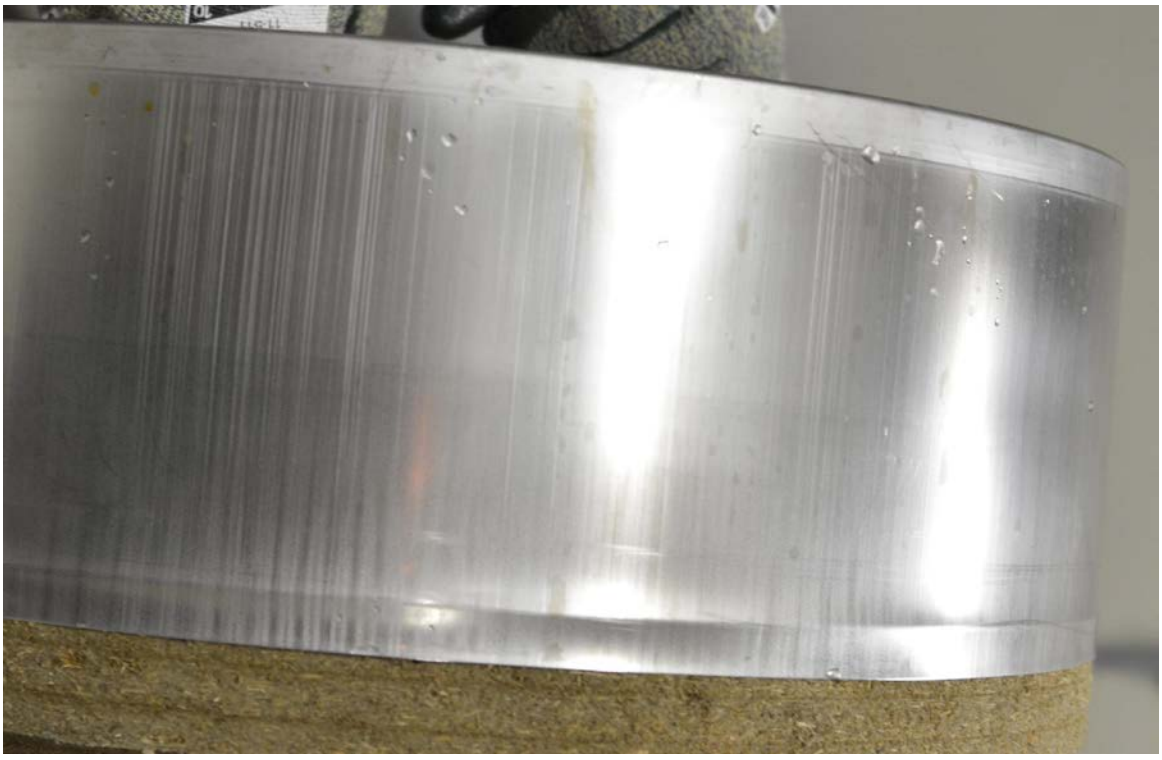

(b)

Figure 3. Water droplets on the underside of the lid (a) and on the side of the air shield (b). Photographs taken by KAC personnel during field surveillance.

Figure 4. Mold on the side of the lower fiberboard subassembly, primarily visible as white lines along the glue joints.

Figure 5. Dark staining (water marks) on the bottom of the lower fiberboard subassembly. In addition, an impression of the step on the bottom of the drum is visible.

Figure 6. ID surface of the lower fiberboard subassembly immediately adjacent to a rectangular feature near the bottom of the lead shield, at about 90 degrees orientation.

Figure 7. ID surface of the lower fiberboard subassembly at about mid-height. The identified band of 3 fiberboard layers has some of the heavier deposits of lead carbonate from the shield at about 315 degrees orientation.

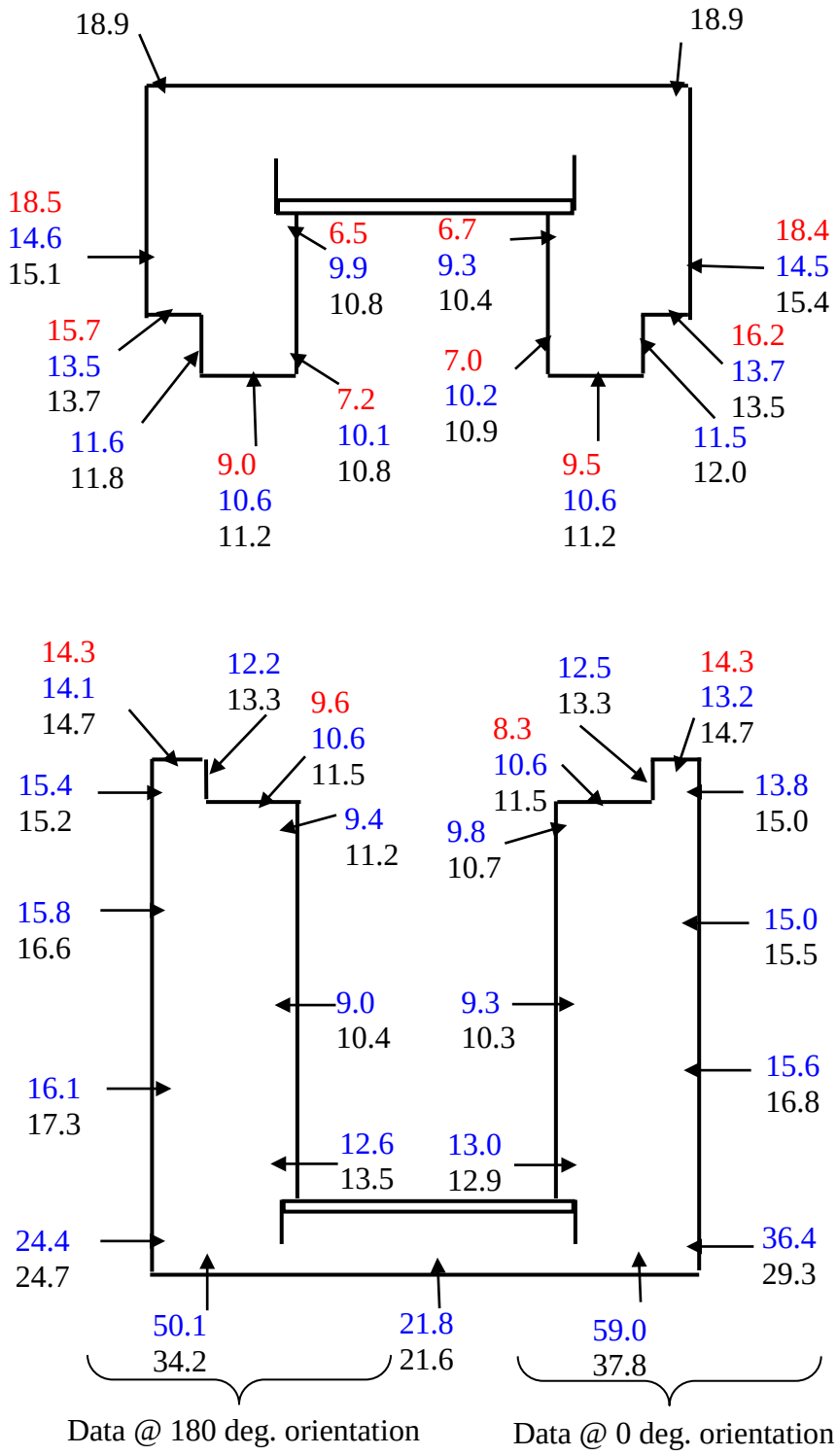

Figure 8. Fiberboard moisture content data. The values in red were measured during field surveillance. The values in blue were measured 27 days later. The **values in black** were measured 40 days after field surveillance. All values are % wood moisture equivalent.

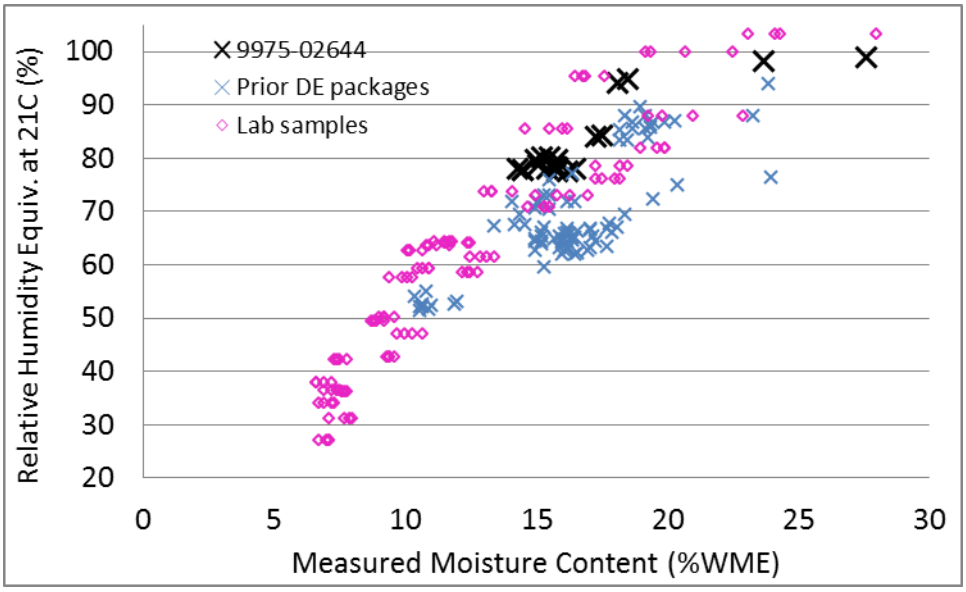

Figure 9. Correlation between fiberboard moisture content and relative humidity of the adjacent air. Data from 9975-02644 are shown with comparable data from prior cane fiberboard DE packages and laboratory samples. Measurements were taken along the fiberboard OD surface. Since relative humidity is temperature dependent, all the data in this graph have been converted to a consistent equivalent relative humidity at 21 °C (70 °F).

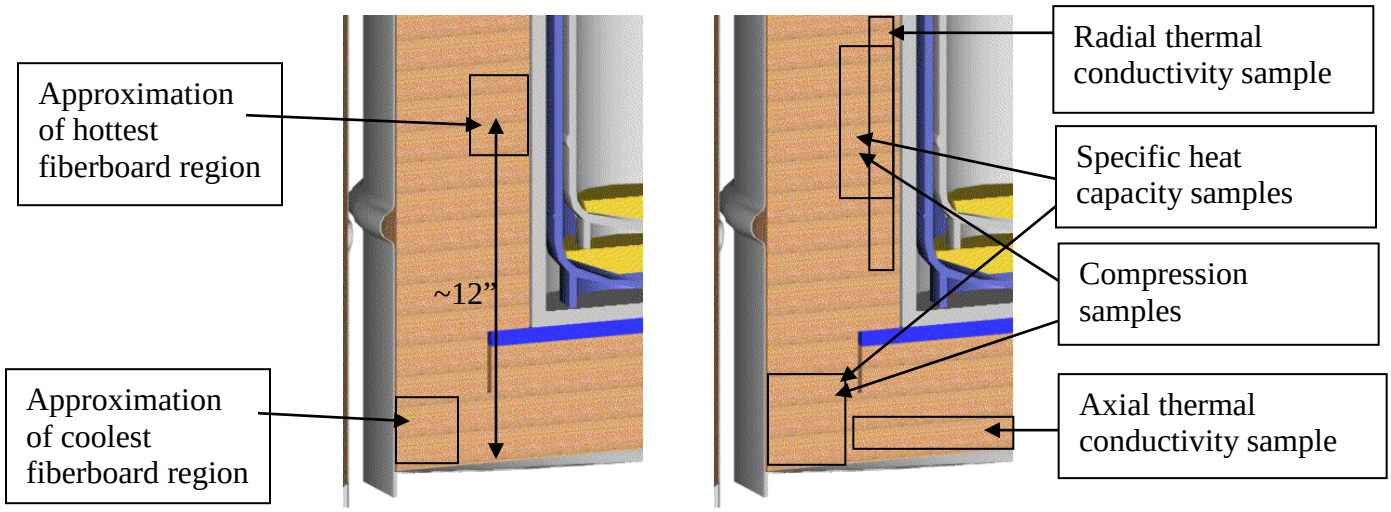

Figure 10. Illustration of fiberboard regions of the lower subassembly to be tested. Multiple samples (where used) were removed from the illustrated locations at different circumferential positions. Not to scale.

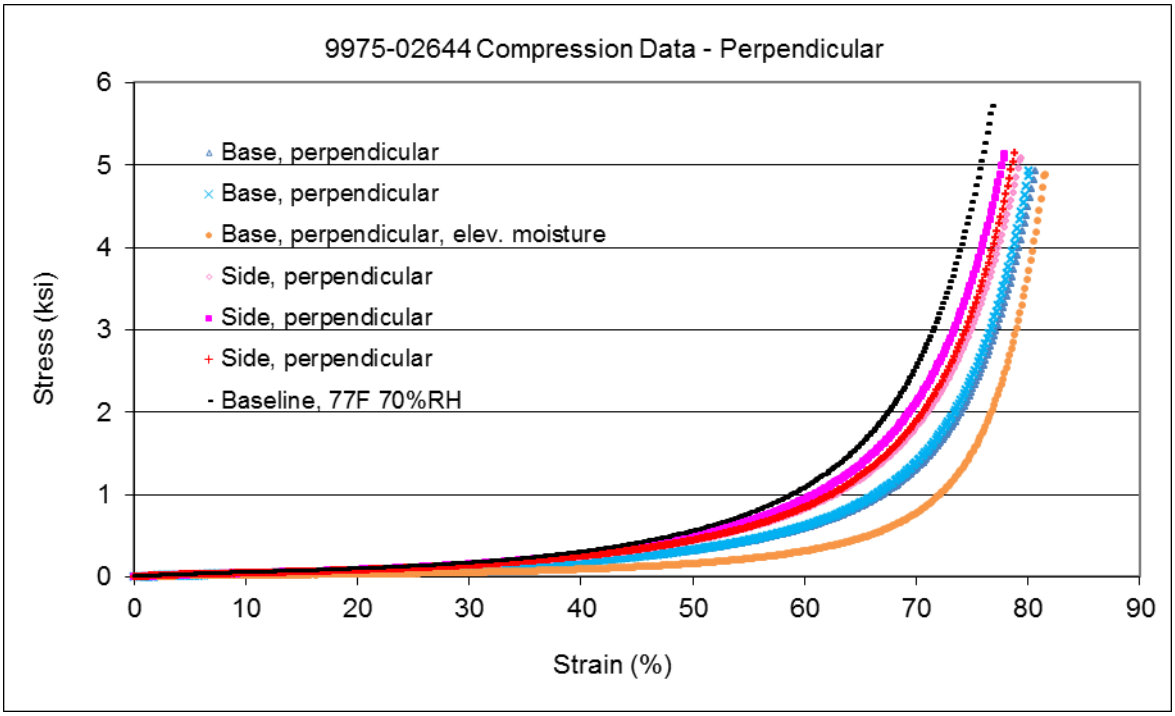

Figure 11. Fiberboard compression test data, compared with typical baseline data from an unaged assembly, in the perpendicular orientation (i.e. load applied perpendicular to the fiberboard layers).

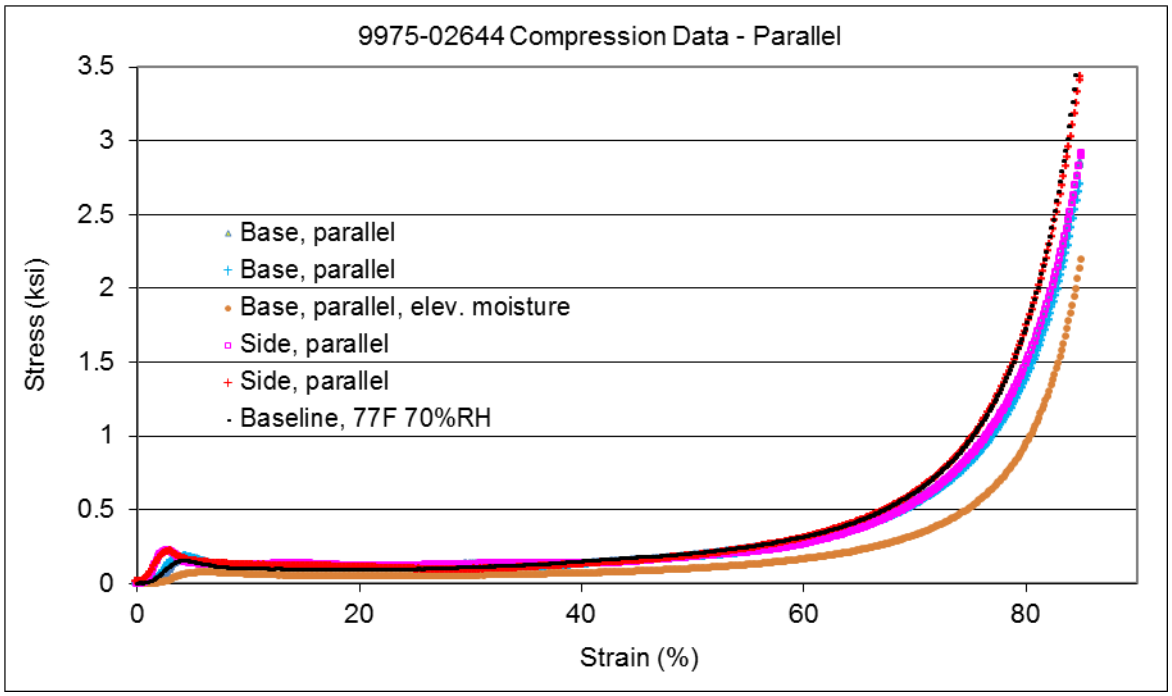

(a)

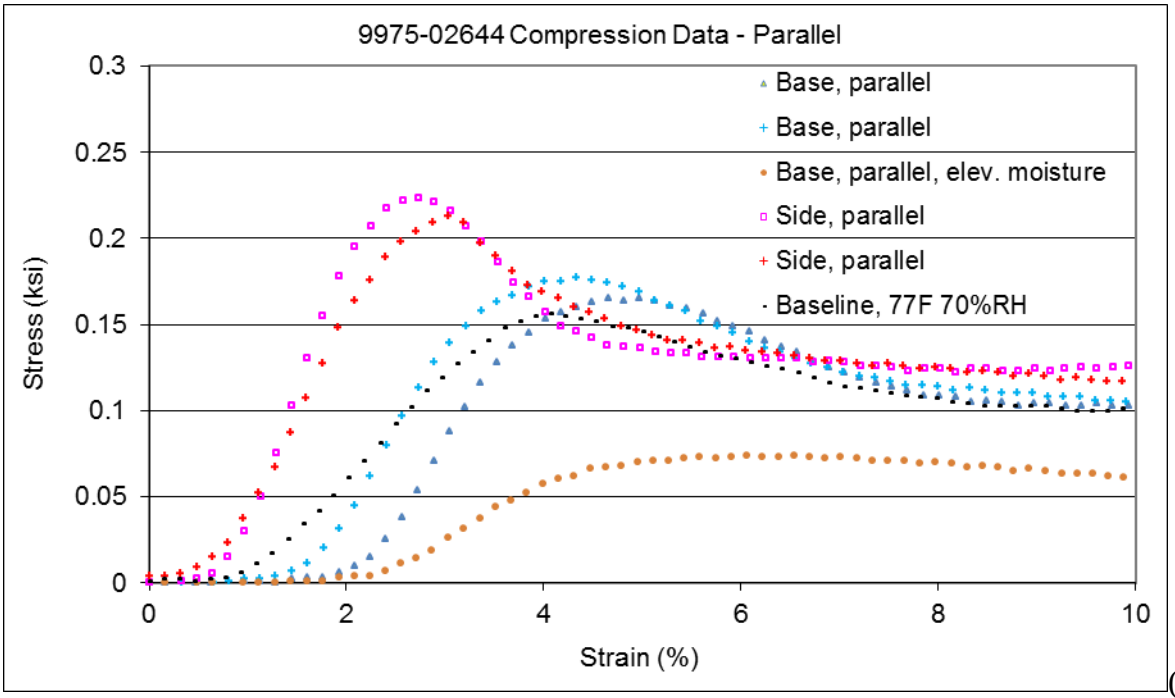

(b)

Figure 12. Fiberboard compression test data, compared with typical baseline data from an unaged assembly, in the parallel orientation (i.e. load applied parallel to the fiberboard layers). The full curves are shown in (a), while the initial buckling region is expanded in (b).

(a) Sample B2 from base of subassembly (b) Sample S1 from side of subassembly

Figure 13. Photographs of fiberboard samples during compression testing, parallel orientation

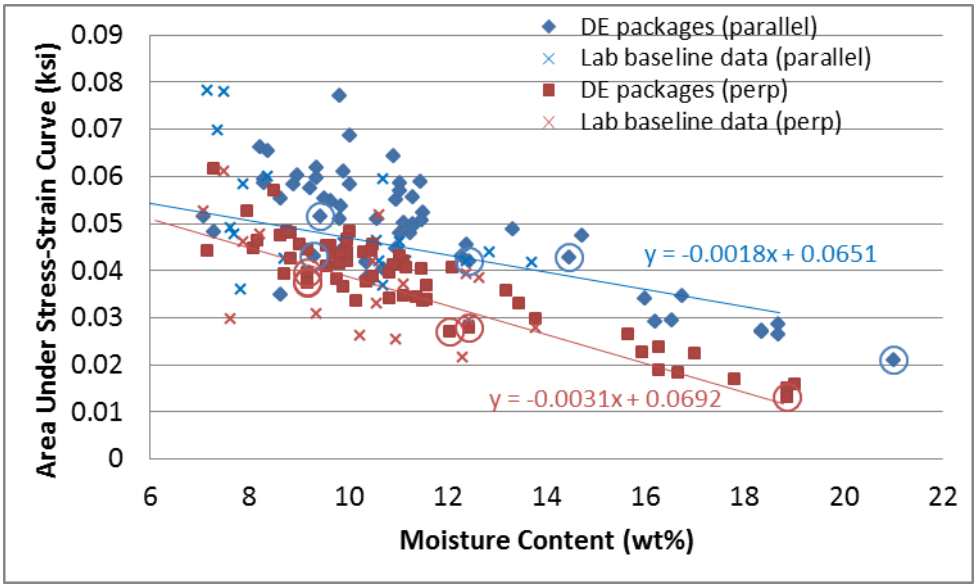

Figure 14. Fiberboard energy absorption, represented by the area under the stress-strain curve up to 40% strain, from compression test samples from all destructively examined packages, compared to baseline data from laboratory samples used to develop fiberboard degradation models. The trendlines represent the laboratory sample data. The results from 9975-02644 are circled.

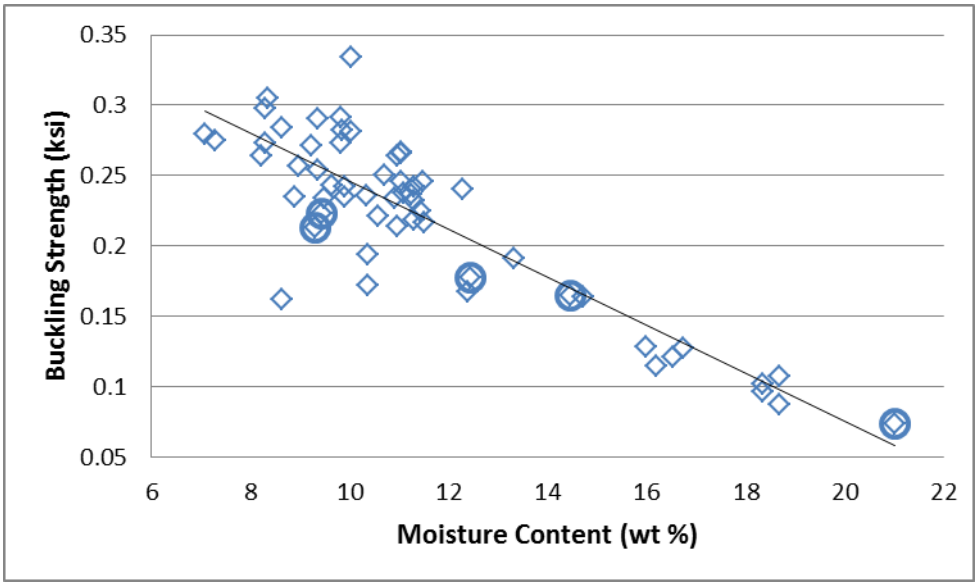

Figure 15. Fiberboard buckling strength for parallel orientation compression test samples from all destructively examined packages. The results from 9975-02644 are circled.

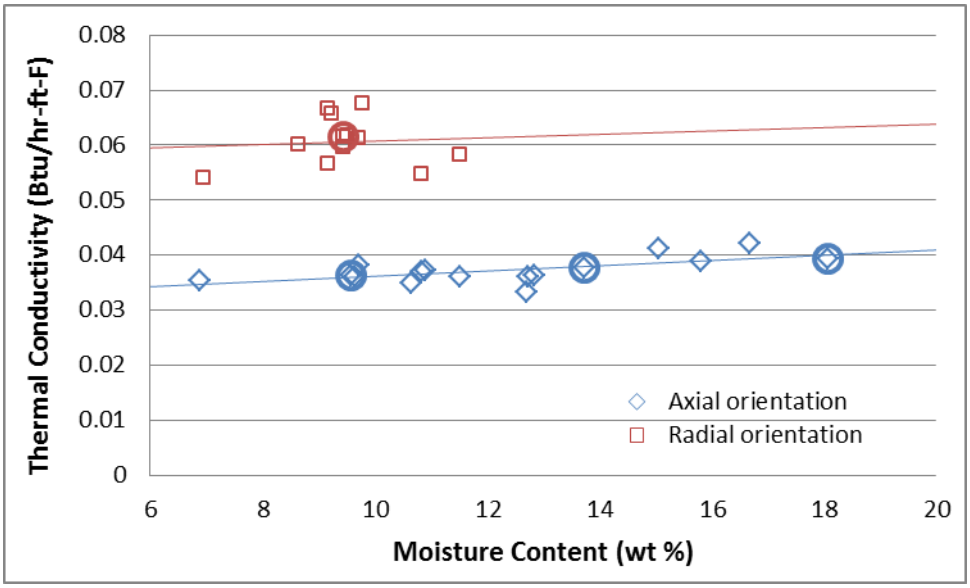

Figure 16. Fiberboard thermal conductivity from all destructively examined packages. The results from 9975-02644 are circled.

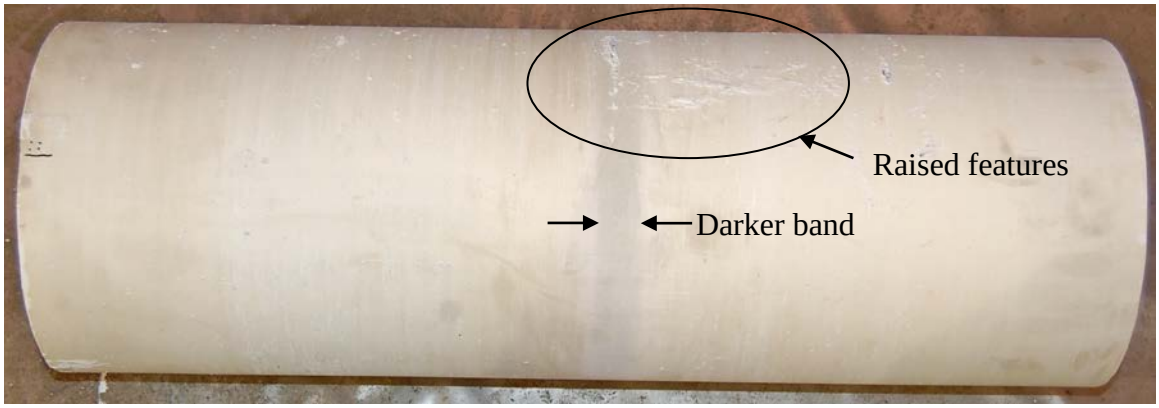

(a) side view

(b) bottom view

Figure 17. Lead shield with white corrosion product. Note the darker band on the side, which corresponds to a lighter colored band of three layers in the lower fiberboard subassembly (see Figure 7). The raised features on and below this band (at ~315 degree orientation) correspond to indentations and transferred corrosion product in the lower fiberboard assembly.

Figure 18. Anomalous feature on the side of the shield at about 90 degrees orientation, corresponding to the lower fiberboard subassembly region shown in Figure 6.

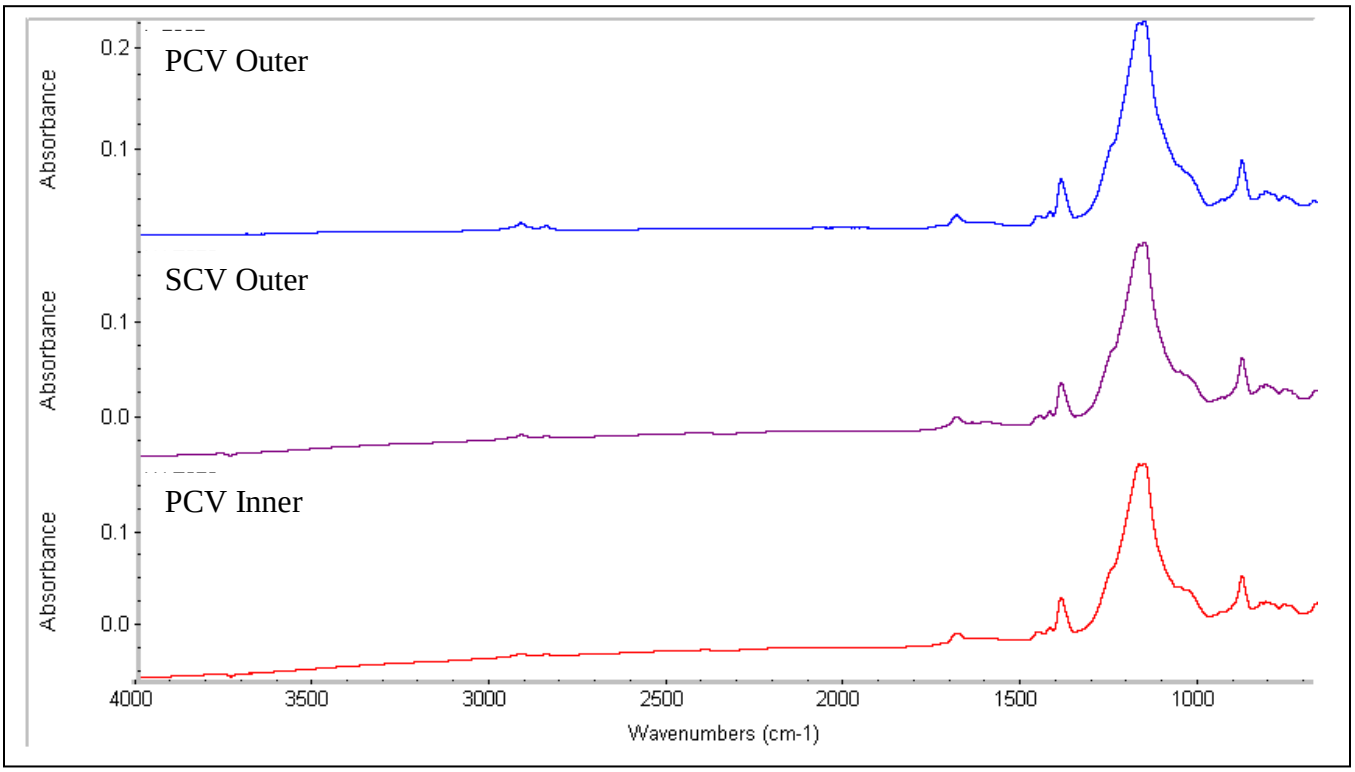

Figure 19. FT-IR spectra for the three tested Viton® GLT O-rings from 9975-02644.

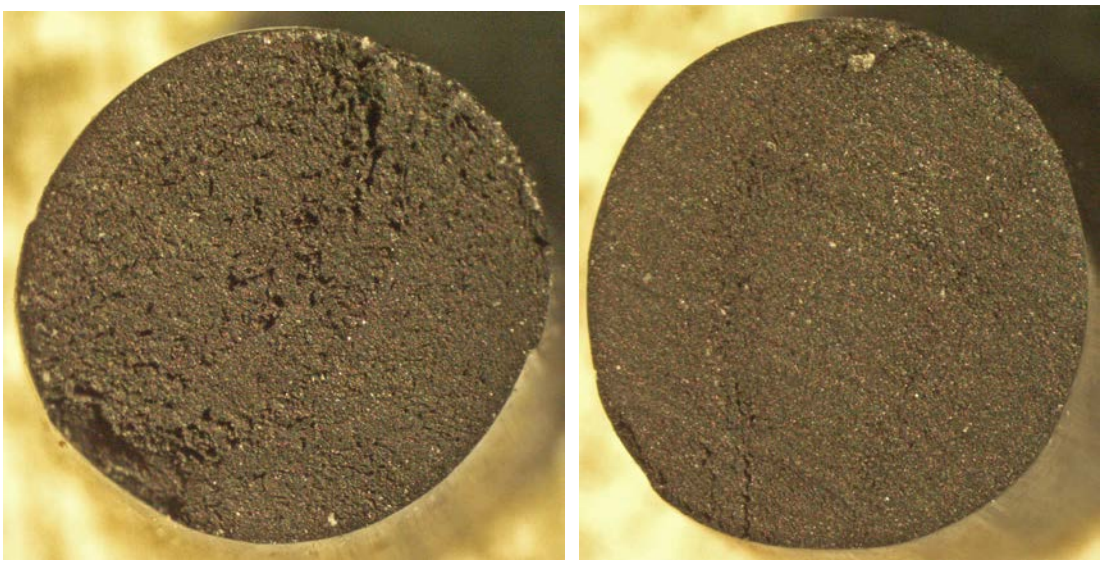

(a) (b)

Figure 20. Optical cross section of the (a) PCV outer and (b) SCV outer O-rings. Photos taken by 723-A Met Lab.

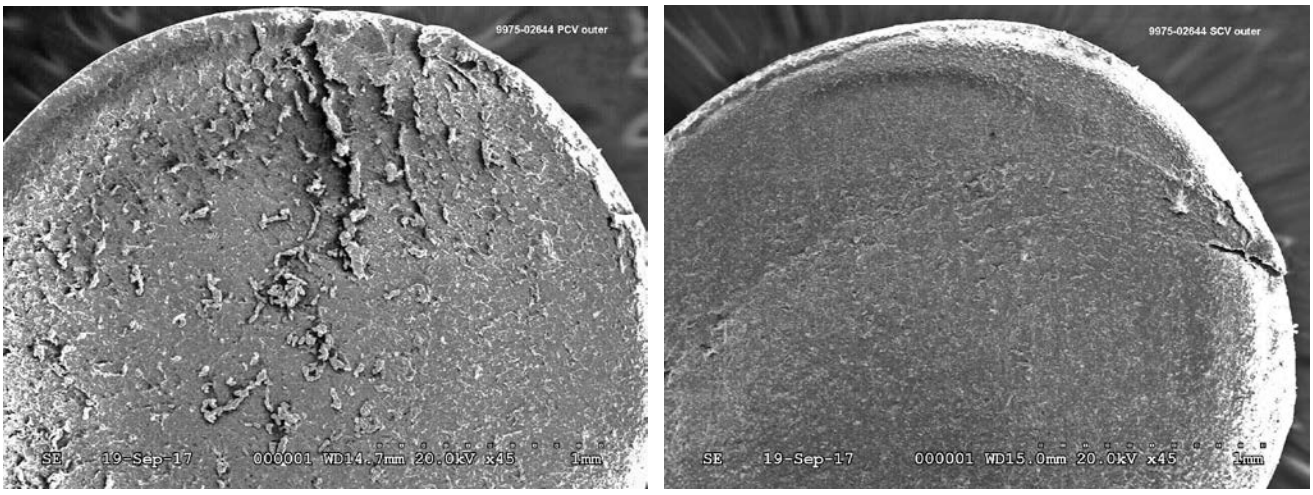

(a) (b)

Figure 21. SEM cross section of the (a) PCV outer and (b) SCV outer O-rings. Photos taken by 723-A Met Lab.

(a) With yarn grips

(b) with flat grips

Figure 22. 9975-02644 PCV inner O-ring during tensile test, at 50% stretch.

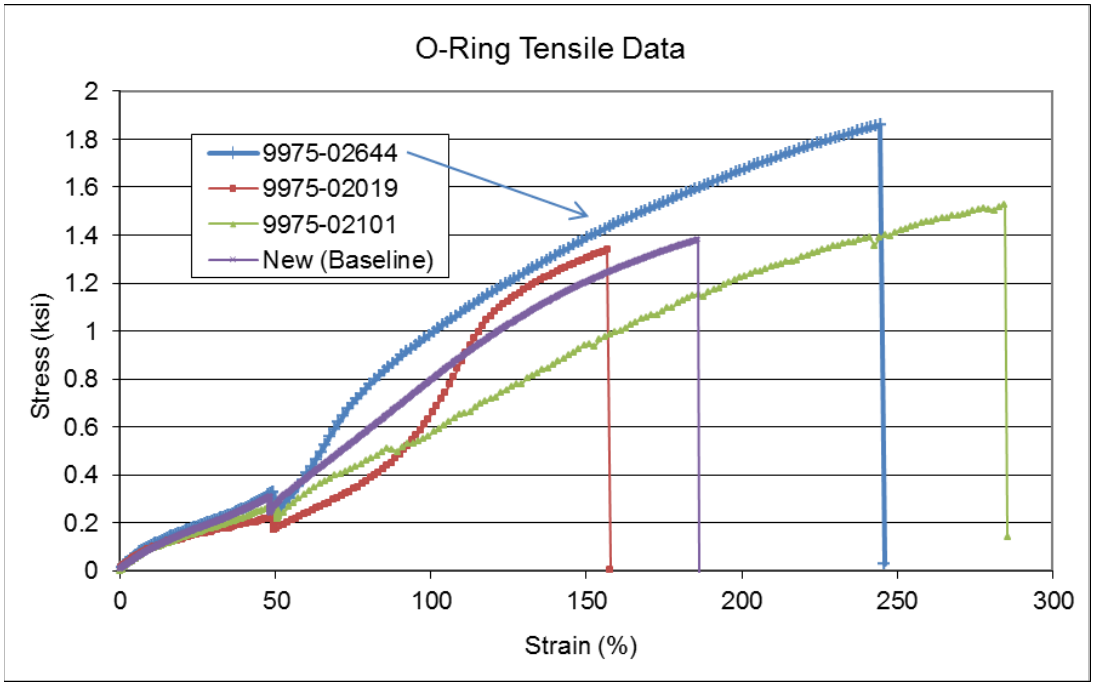

Figure 23. Tensile data for PCV inner O-ring from 9975-02644, with comparison curves from other DE packages with Viton GLT O-rings. Each of these tests was conducted with the flat grip configuration.


(a)


(b)


(c)

Figure 24. Corrosion along the bottom rolled edge of the drum at approximately 110° (a), 210° (b) and 340° (c) orientations

Figure 25. Corrosion along the crevice between the bottom rolled edge and the OD side of the drum, at about 30° orientation

Figure 26. Corrosion on the OD side of the drum at about 170° orientation

Figure 27. Small spots of corrosion along the bottom corner of the drum at about 270° orientation

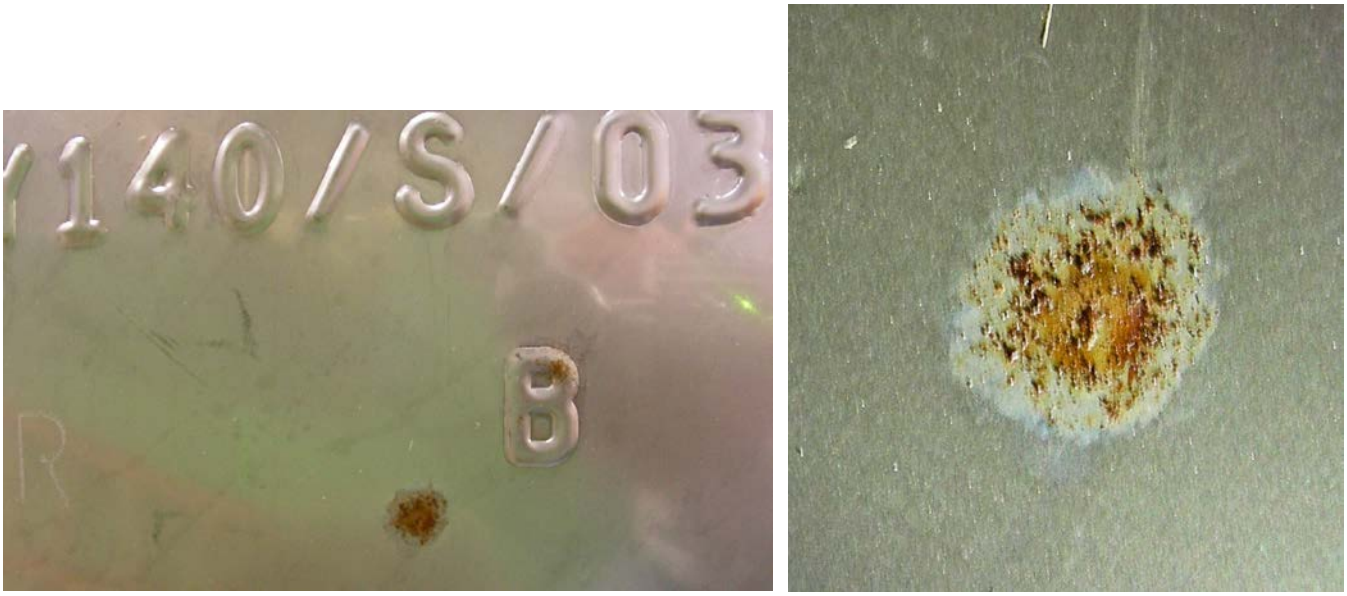

(a) (b)

Figure 28. Corrosion on the bottom of the drum (a), with close-up in (b)

Figure 29. Corrosion spot on the drum bottom after the corrosion product was removed, showing numerous small pits.

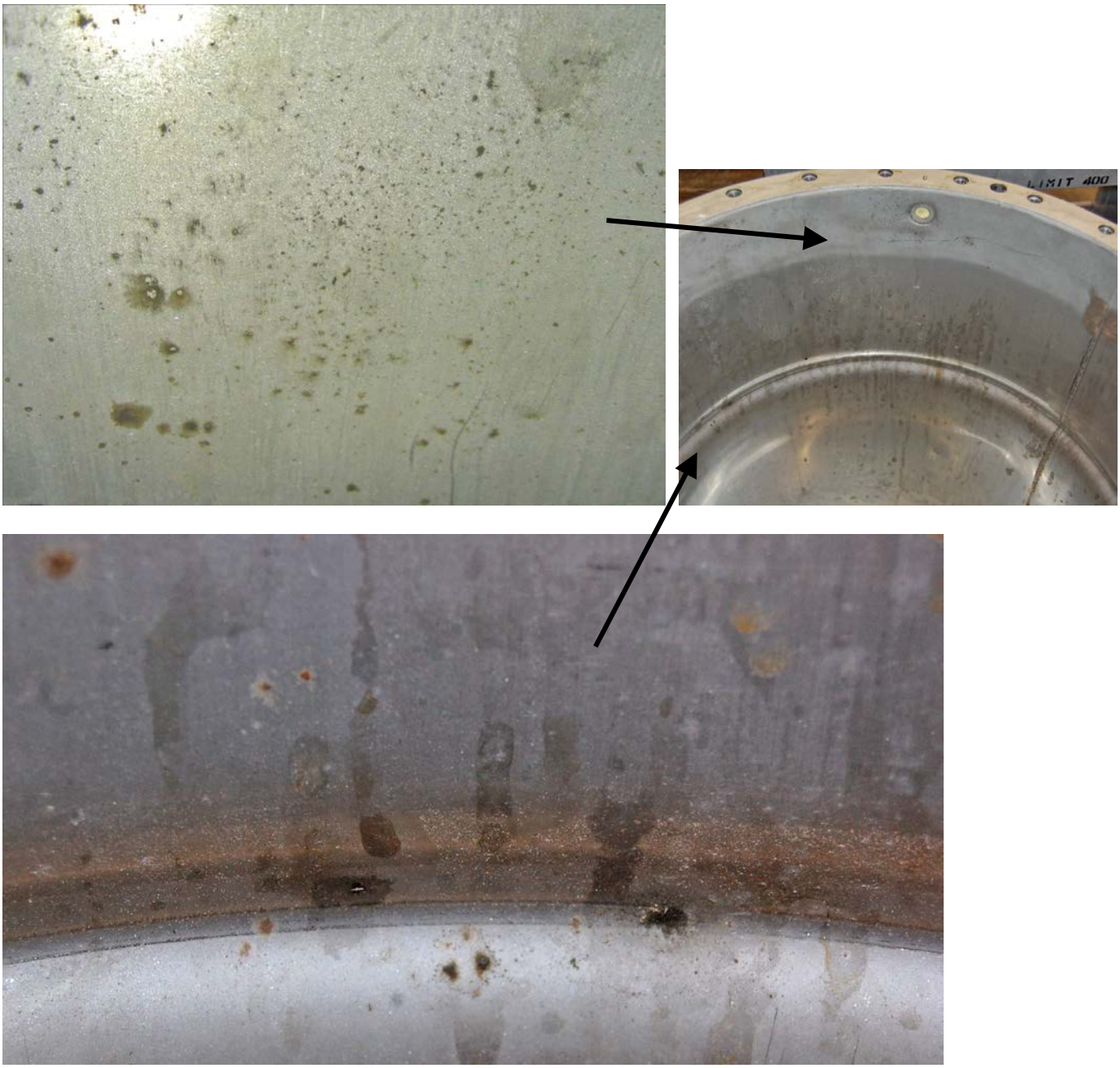

Figure 30. Corrosion and water staining on the drum interior surface, near 0° orientation

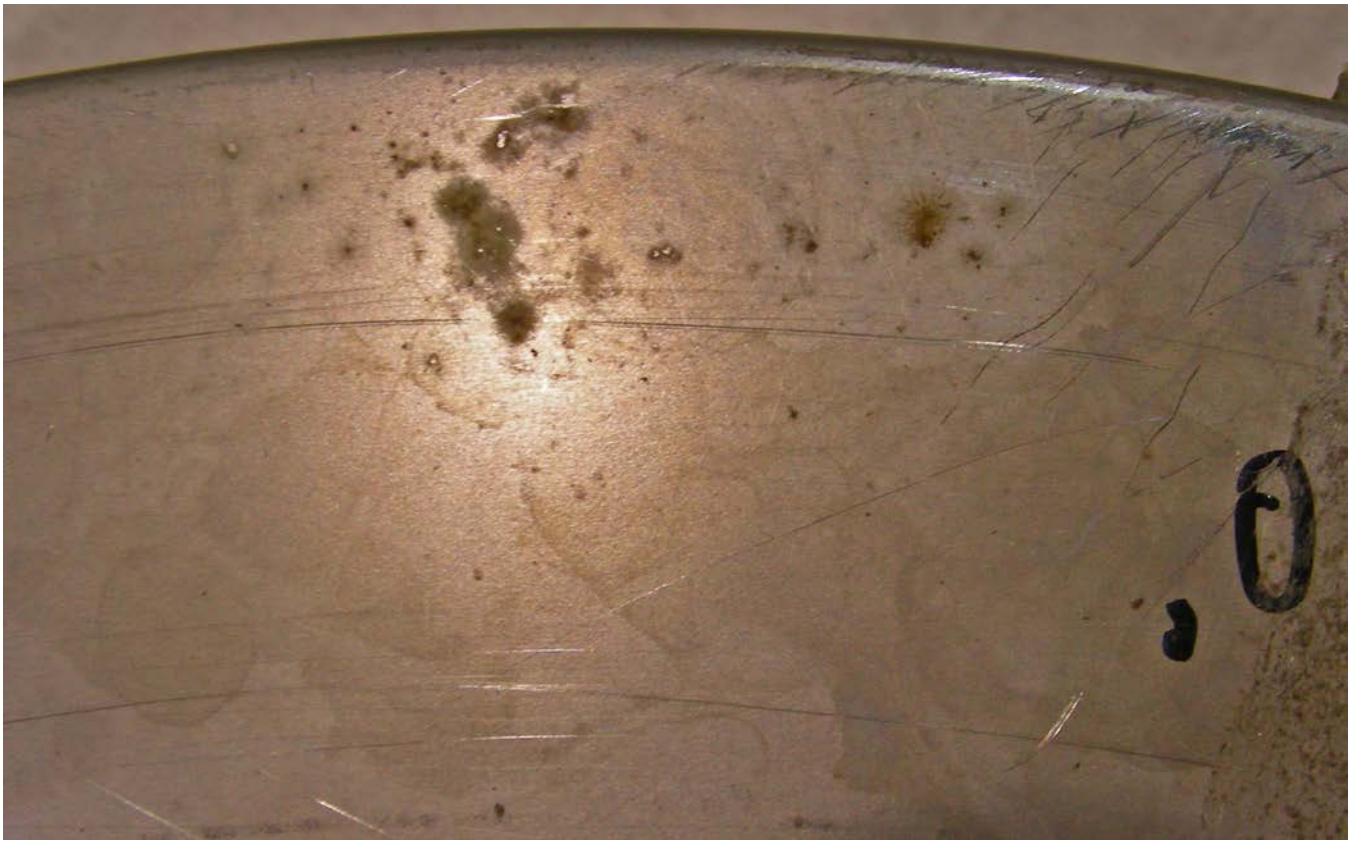

Figure 31. Corrosion on the air shield near the 0° orientation

Attachment 1 9975-02644 Field Surveillance Results, with Comparison to Destructive Examination Results

Section I

Drum Exterior Examination

Item	Field Surveillance Result	Destructive Exam. Result
Drum vent plugs are specified and are in place as required	SAT	SAT
Drum surface is not dented beyond 0.25 inch	SAT	SAT
Drum Dents adjacent to the air shield are not deeper than 0.125 inch	SAT	SAT
Drum surface is free from corrosion, swelling/bulging and other physical damage	SAT	UNSAT

Comment – Several small corrosion spots along the bottom lip of drum and just above the bottom lip (exterior) during DE exam. Patches of corrosion observed on drum ID surface among numerous water stains during DE exam. Photos of these features were taken during field surveillance, but neither was noted on the data sheet.

Section II

Humidity Measurements

Humidity at top of the drum 98.4 %RH 57.1 %RH on 8/2/17

Section III

Temperature Measurements

[These data not repeated in this report.]

Section IV

Celotex® Inspection

Upper Celotex® Assembly Weight: 26.6 lb (field surv.) 12.097 kg / 26.67 lb (destructive exam)

Visual:

Item	Field Surveillance Result	Destructive Exam. Result
Inspect all exposed Celotex® surfaces for significant damage and ensure layers are well bonded	SAT	SAT
Upper Celotex® came out smoothly, without interference	SAT	SAT
All visible Celotex® surfaces are free from staining and variation in coloration	SAT	UNSAT
Celotex® is free from significant swelling (e.g. gap exists against drum), shrinkage and other significant physical damage	SAT	SAT
Lead shield is free from significant deformation and physical damage and shows no sign of flaking, blistering or spalling	SAT	SAT
Lead shield Go/No Go gauge went smoothly into the lead shield and reached all the way to the bottom of the lead shield	SAT	NA

Comments: From field surveillance, “Water droplets noted on underside of drum lid and on top of thermal blanket upon initial opening” From DE: “Evidence of mold (now apparently inactive) along some of the lowest glue joints of the lower assembly. A moderate musty odor was noted when the lower assembly was removed.”

Attachment 1 9975-02644 Field Surveillance Results, with Comparison to Destructive Examination Results

Celotex® Dimensions (all results reported in inches)

Dimensions		0°	90°	180°	270°	Field Surveillance Average	Destructive Exam. Average
1	Upper Assembly OD	17.632	17.628			17.630	17.646
2	Upper Assembly lower step OD	14.672	14.652			14.662	14.696*
3	Upper Assembly ID	8.540	8.544			8.542	8.563
4	Upper Assembly inside height	4.991	4.991	4.992	4.954	4.982	5.004
5	Lower Assembly step height	1.995	1.995	1.996	2.000	1.997	2.004
6	Lower Assembly height from lower step to top of lead shield	4.648	4.669	4.678	4.683	4.669	NA

* calculated value

Dimension	Result	Criteria	Field Surveillance Result	Destructive Exam. Result
Dimension #4 average – Dimension #6 average	0.299	>0.425”	UNSAT	NA
Dimension #6 average	4.669	$\leq$ 4.65 ”	SAT	NA
Dimension #1 average – Dimension #3 average	9.088	$\geq$ 8 3/16 ”	SAT	SAT

Section V

O-Ring Inspection

Test	SAT/UNSAT
O-ring seal test performed on SCV	SAT
SCV O-rings were removed intact	SAT
SCV O-rings have no excess accumulation of grease	SAT
O-ring seal test performed on PCV	SAT
PCV O-rings were removed intact	
PCV O-rings have no excess accumulation of grease	

Comments: n/a

Attachment 1 9975-02644 Field Surveillance Results, with Comparison to Destructive Examination Results

(all dimensional results reported in inches)

Action	0°	90°	180°	270°	Time	Destructive Exam. Average Result
Loosen SCV lid					0941	NA
Outer SCV O-Ring						
Measure OD (while on plug)	6.299	6.302			0948	NA
Measure radial thickness	0.1275	0.1285	0.1355	0.1355	0950	0.1389
Measure vertical thickness	0.1365				0950	0.1337
Inner SCV O-Ring						
Measure OD (while on plug)	6.182	6.188			0949	NA
Measure radial thickness	0.1240	0.1240	0.1250	0.1260	0951	0.1308
Measure vertical thickness	0.1350				0951	0.1366
Loosen PCV lid					1009	NA
Outer PCV O-Ring						
Measure OD (while on plug)	5.253	5.254			1010	NA
Measure radial thickness	0.1275	0.1270	0.1265	0.1310	1018	0.1358
Measure vertical thickness	0.1365				1017	0.1354
Inner PCV O-Ring						
Measure OD (while on plug)	5.142	5.135			1016	NA
Measure radial thickness	0.1365	0.1255	0.1370	0.1370	1020	0.1384
Measure vertical thickness	0.1305				1019	0.1334

Attachment 1 9975-02644 Field Surveillance Results, with Comparison to Destructive Examination Results

SRNL Receipt Examination of O-Rings

VISUAL EXAMINATION

PCV	PCV Outer	PCV Inner
Grease present	yes	yes
Color (normal or explain)	Normal	Normal
Cross-sectional shape	round	round
Nicks, Scratches, Cracks	Bubbles on seam	none
Other Damage (Note extent/size)	none	none
Picture (Note if taken)		

SCV	SCV Outer	SCV Inner
Grease present	yes	yes
Color (normal or explain)	Normal	Normal
Cross-sectional shape	round	round
Nicks, Scratches, Cracks	none	none
Other Damage (Note extent/size)	none	none
Picture (Note if taken)		

THICKNESS (all results reported in inches)

PCV	PCV Outer		PCV Inner	
	Axial	Radial	Axial	Radial
Thickness 1 (in)	0.1360	0.1325	0.1325	0.1315
Thickness 2 (in)	0.1335	0.1370	0.1325	0.1380
Thickness 3 (in)	0.1375	0.1405	0.1340	0.1405
Thickness 4 (in)	0.1375	0.1340	0.1385	0.1350
Field Surv. Average	**0.1361**	**0.1360**	**0.1344**	**0.1363**
Destructive Exam Average	**0.1354**	**0.1358**		

SCV	SCV Outer		SCV Inner	
	Axial	Radial	Axial	Radial
Thickness 1 (in)	0.1370	0.1325	0.1370	0.1295
Thickness 2 (in)	0.1360	0.1320	0.1370	0.1295
Thickness 3 (in)	0.1280	0.1365	0.1360	0.1300
Thickness 4 (in)	0.1360	0.1365	0.1360	0.1305
Field Surv. Average	**0.1343**	**0.1344**	**0.1365**	**0.1299**
Destructive Exam Average	**0.1337**	**0.1389**		

Attachment 1 9975-02644 Field Surveillance Results, with Comparison to Destructive Examination Results

SRNL Receipt Examination of O-Rings (Continued)

HARDNESS

	PCV O-Rings		SCV O-Rings	
	Outer	Inner	Outer	Inner
Hardness 1, M-Scale	72.5	70.5	71.0	77.5
Hardness 2, M-Scale	74.0	74.0	69.0	78.0
Hardness 3, M-Scale	74.0	73.0	76.0	75.0
Hardness 4, M-Scale	70.5	71.5	76.0	78.0
Hardness 5, M-Scale	72.0	71.0	70.0	77.0
Average	**72.6**	**72.0**	**72.4**	**77.1**

CONTINUATION:
NA

CC: R. J. Bayer, 705-K
J. S. Bellamy, 730-A
W. L. Daugherty, 773-A
B. L. Garcia-Diaz, 999-2W
T. W. Griffin, 705-K
T. J. Grim, 105-K
R. J. Grimm, 705-K
E. R. Hackney, 703-H
S. J. Hensel, 705-K
J. M. Jordan, 705-K
B. B. Kiflu, 705-K
D. R. Leduc, 730-A
P. L. Livengood, 705-K
J. W. McEvoy, 730-A
M. M. Reigel, 773-A
T. E. Skidmore, 730-A
D. E. Welliver, 705-K
K. E. Zeigler, 773-41A
Document Control